

Impact of urban imperviousness on boundary layer meteorology and air chemistry on a regional scale

JOACHIM FALLMANN^{1,2,3*}, MARC BARRA³, VINOD KUMAR⁴ and HOLGER TOST³

¹South German Climate Office, Institute of Meteorology and Climate Research, Karlsruhe Institute of Technology, Germany

²Institute of Meteorology and Climate Research – Tropospheric Research, Karlsruhe Institute of Technology, Germany

³Institute of Atmospheric Physics, Johannes Gutenberg University Mainz, Germany

⁴Max Planck Institute for Chemistry, Mainz, Germany

(Manuscript received February 1, 2021; in revised form April 20, 2021; accepted April 21, 2021)

Abstract

It has been long understood that land cover change from natural to impervious modifies the surface energy balance and hence the dynamical properties of the overlying atmosphere. The urban heat island is manifested in the formation of an urban boundary layer with distinct thermodynamic features that in turn govern transport processes of air pollutants. While many studies already demonstrated the benefits of urban canopy models (UCM) for atmospheric modelling, work on the impact on urban air chemistry is scarce. This study uses the state-of-the-art coupled chemistry-climate modelling system MECO(n) to assess the impact of the COSMO UCM TERRA_URB on the dynamics and gas phase chemistry in the boundary layer of the urban agglomeration Rhine-Main in Germany. Comparing the model results to ground observations and satellite and ground based remote sensing data, we found that the UCM experiment reduces the bias in temperature at the surface and throughout the boundary layer. This is true for ground level NO₂ and ozone distribution as well. The application of MECO(n) for urban planning purposes is discussed by designing case studies representing two projected scenarios in future urban planning – densification of central urban areas and urban sprawl. Averaged over the core urban region and 10-days during a heat wave period in July 2018, model results indicate a warming of 0.7 K in surface temperature and 0.2 K in air temperature per 10 % increase in impervious surface area fraction. Within this period, a 50 % total increase of imperviousness accounts for a 3 K and 1 K spatially averaged warming respectively. This change in thermodynamic features results in a decrease of surface NO₂ concentration by 10–20 % through increased turbulent mixing in areas with highest impervious fraction and highest emissions. In the evening and nighttime however, increased densification in the urban centre results in amplified canyon blocking, which in turn results in average increase in near surface NO₂ concentrations of about 10 %, compared to the status quo. This work intends to analyse regional scale features of surface-atmosphere interactions in an urban boundary layer and can be seen as preparatory work for higher resolution street scale models.

Keywords: Urban air quality, urban planning, boundary layer, heat wave, regional scale, urban canopy parametrization

1 Introduction

Urbanization involves the transfer from natural land into impervious surface, which is manifested by a loss of vegetation cover, and natural soil functions. Between 2012–2017 global urban impervious cover increased from 24.3 % to 25.9 % (NOWAK and GREENFIELD, 2020). In Europe, on average 1.414 % of the total land area was sealed in 2006, while this increased to 1.481 % in 2015. Sealed area in Germany has been increased from 4.18 % in 2006 to 4.31 % in 2015 (UMWELTBUNDESAMT, 2019). With climate extremes such as hot days or tropical nights most likely to increase in the future, globally

(MUELLER and SENEVIRATNE, 2012), regionally (BENISTON et al., 2007; GEORGESCU et al., 2013; JONES et al., 2015; FALLMANN et al., 2017) and locally (SCHAU-NOPPEL et al., 2020), particularly urban dwellers residing in large metropolitan areas will be facing increased danger by intensifying heat waves. Climate change in cities is aggravated by specific urban effects e.g. by heat trapping caused by the building morphology (HAYHOE et al., 2010; MCCARTHY et al., 2010; CARVALHO et al., 2017; SHARMA et al., 2019; SCHAU-NOPPEL et al., 2020). Analysing projections of different development plans for urban areas in North-West Germany, (STROHBACH et al., 2019) found, that an increase of impervious surface area by 55 % would account for an increase of 19 % in surface runoff and a decrease of evaporation of 1 %. In their study, they further stated, that a population increase in that area by 7 % from 1980 to 2015 resulted

*Corresponding author: Joachim Fallmann, Karlsruher Institut für Technologie (KIT), Institut für Meteorologie und Klimaforschung, Postfach 3640, 76021 Karlsruhe, Germany, e-mail: joachim.fallmann@kit.edu

in an increase of impervious surface area by 34 % in the same period. The 3-dimensional nature of the urban canopy involves an increase of the total surface area that is sealed and leads to trapping of heat within street canyons. Natural ventilation is hampered and heating further accelerated. That aspect is amplified during calm and stationary meteorological conditions, predominately found during heat wave periods which are projected to increase in the future (McCARTHY et al., 2010; TRIMMEL et al., 2021).

Assessing the living quality of urban areas however involves, next to social, political and economic factors the quality of urban air (HEWITT et al., 2020). Road transport is one of Europe's main sources of air pollution (GONZALES-ORTIZ, 2019). Hence, NO₂ remains one of the most severe pollutants in European urban areas (LORENTE et al., 2019), causing danger to human health directly (ACHAKULWISUT et al., 2019) or via secondary production of ozone, particulates or acid rain (KELLY, 2019). Left alone emission control itself, the residence time of pollutants within an urban entity is governed by its morphology. (XIE et al., 2005). Buildings act as roughness elements, absorbing momentum and reduce the turbulent intensity of the airflow. In the distinct urban roughness sub-layer, atmospheric turbulence breaks down and the effective transport velocity scale is reduced. Hence, the transport and vertical dilution of pollutants emitted at the surface is hampered and resistance time inside the canyon is increased.

The impact of urban boundary layer dynamics on air pollution levels however is further controlled by thermally driven flows arising from changes in the surface properties, e.g. when heat mitigation strategies alter surface sensible heat fluxes (MAKAR et al., 2006; EL-GHAZOUANI et al., 2019). As such, surface cooling, e.g. by using reflective coatings or green infrastructure can have adverse effects on air quality through alteration of lower atmosphere dynamics, including reduced vertical mixing and a lower boundary layer depth (FALLMANN et al., 2017; SHARMA et al., 2019). In turn, destabilization of urban air over intense urban heat islands lead to local formation of convective boundary layers which can result in a near surface reduction of the total mass of air pollutants (LEUKAUF et al., 2016).

With increasing population, the compact city approach has gained global impact in order to allow for sustainable urban growth. Positively that strategy counteracts negative effects arising from extensive land consumption by urban sprawl. On the negative side, denser and compact city structures provide a threat to natural urban spaces (HAALAND and VAN DEN BOSCH, 2015). This study intends to contrast both scenarios, urban compaction and urban sprawl based on their impact on urban heat and air pollution during heat wave conditions for the densely populated central European metropolitan area Rhine-Main. Recent studies indicate that the number of hot days (with daily maximum air temperature exceeding 30 °C) is projected to increase from 21 (1971–2000) to 27 (2031–2060) in that area – refer-

ring to the maximum value of an urban grid cell with 100 × 100 m extracted from downscaled regional climate simulations (SCHAU-NOPPEL et al., 2020).

July 2018 serves as reference case for model simulations in this work as it represents a particular dry and hot period. With regard to air quality, the critical annual mean value of NO₂, which is relevant for human health (larger than 40 µg m⁻³ on yearly average) is exceeded at urban measurement locations within the study area (Ludwigshafen-Heinigstraße: 41 µg m⁻³, Mainz-Parcusstraße: 48 µg m⁻³, Koblenz-Hohenfelder Str.: 40 µg m⁻³). During the case study period July, the monthly mean concentrations accounted for 40 µg m⁻³, 48 µg m⁻³ and 42 µg m⁻³ respectively (LANDESAMT FUER UMWELT RHEINLAND PFALZ, 2018). While µg m⁻³ is the European standard, for model evaluation and experiments, all concentrations will be expressed in parts per billion (ppb), using a conversion factor 1 ppb = 1.88 µg m⁻³ (DEFRA, 2005). Two scenarios of expected urban developments are executed, using the state-of-the-art coupled chemistry-climate modelling system MECO(n) (KERKWEG and JÖCKEL, 2011; HOFMANN et al., 2012; KERKWEG and JÖCKEL, 2012; MERTENS et al., 2016) at high resolution, coupled to the COSMO-CLM urban canopy parametrization (WOUTERS et al., 2016b). The latter is an urban upgrade of the standard soil module of COSMO-CLM TERRA (GRASSELLT et al., 2008) originally used in MECO(n). Mesoscale meteorology has been evaluated for MECO(n) by (HOFMANN et al., 2012), while (MERTENS et al., 2016), provided a chemical evaluation for ozone on a European domain. COSMO-CLM/TERRA_URB is already evaluated for other cities (e.g. Berlin (TRUSILOVA et al., 2016)) but to the authors knowledge it has not been applied to regional or urban air quality investigations. Due to its low computational extra cost, following results from TRUSILOVA et al. (2016) TERRA_URB is recommended for simulating surface to boundary interactions on a regional scale.

The manuscript is structured as followed. First, the model setup is explained based on the selection of the case study period, model domain and configuration of the dynamical setup and chemical mechanisms used. A detailed evaluation of MECO(n) with regard to meteorology and air quality for both surface and boundary layer follows. In the next chapter, two urban planning scenarios are compared in terms of temperature and NO₂ concentration followed by a discussion. Addressing model results, the suitability of the term urban heat island for assessing heat mitigation strategies in urban areas is analysed referring to (MARTILLI et al., 2020) in the appendix.

2 Model and methods

2.1 Study area and meteorological conditions

During stationary weather conditions, with weak synoptic forcing, urban heat islands are most pronounced,

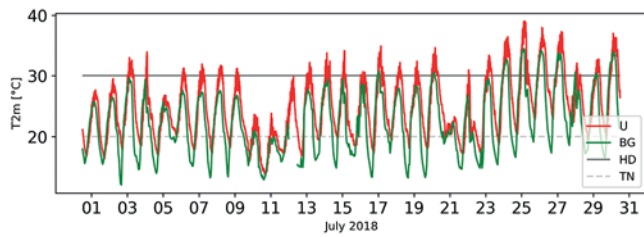


Figure 1: Time series of 2 m temperature observed in the urban centre (U) and the urban background (BG). Threshold for hot days (HD) and tropical nights (TN) are marked in black and grey dotted.

especially at night. In these conditions, differences in imperviousness lead to small differences of the energy balance, modifying the thermodynamic structure of the urban boundary layer. The Frankfurt Rhine-Main metropolitan area (abbreviated FRM) approximately covers an area of about 14800 km² and shares a population of about 5.2 million people. The main urban centres that are in the focus of this study are the capital cities of Rhineland-Palatinate (Mainz) and of Hessian (Wiesbaden), the city of Frankfurt in the East and the urban agglomeration Mannheim, Heidelberg, Ludwigshafen to the South. According to Corine land use classification 2018 (BUETTNER, 2004) the percentage of areas classified as either continuous, discontinuous urban fabric or industrial and commercial account for 70 %, averaged over the municipal areas of the above-mentioned places. With annual exceeding air quality standards of NO₂, this area suffers from high air pollution and climate change additionally aggravates the well-being of urban dwellers (SCHAU-NOPPEL et al., 2020).

In the first half of July 2018, dry and continental air masses reached the FRM-area from Eastern Europe and favoured the onset of a stable high-pressure system. In the second half of that month, the synoptic patterns changed to advection of humid and warm air masses from the South-West reaching the continent. The monthly mean precipitation of 35 l/m² measured for Rhineland-Palatinate was 50 % lower than the climatological mean for July. Referring to long term measurements of the German Weather Service, with 21 °C, the mean July temperature in Rhineland Palatinate was well above the climatological mean (1961–1990) of 17 °C (<https://www.ipa.uni-mainz.de/juli-2018/>). For the reason of representativeness, this value is calculated from a background station and therefore masks temperature extremes emerging in urban areas. With regard to observations in the city centre of Mainz, monthly mean air temperature amounts to 24.6 °C. Regarding observations in the urban background (located west to the campus of the University Mainz (Fig. 1)) only 4 days in July 2018 are not to be counted as summer days, with $T_{\max} > 25$ °C. That sums up to 27 summer days and 11 hot days ($T_{\max} > 30$ °C). No precipitation was recorded until mid of July. 21 hot days have been recorded at an urban measurement station Mainz.

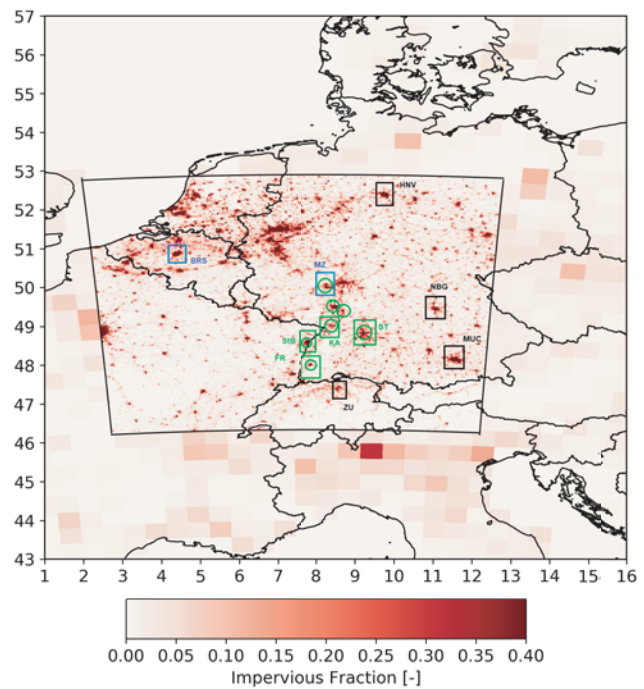


Figure 2: CM_3 domain (3 km) embedded in extracted area of the CM_40 domain (40 km) showing ISA (impervious surface area). Coloured boxes indicate areas relevant for text and Figure A.1 in the appendix.

2.2 Model setup

For this study we applied the MECO(n) (MESSy-fied ECHAM and COSMO models nested n times) model system (KERKWEG and JÖCKEL, 2012a; JÖCKEL et al., 2016; MERTENS et al., 2016). MECO(n) performs a one-way (the coarse domain provides boundary conditions to next smaller) online coupling (every time step of the coarser/driving model instance) between the global earth system model EMAC (JÖCKEL et al., 2010) and the non-hydrostatic regional climate model COSMO-CLM/MESSy (KERKWEG and JÖCKEL, 2012a). COSMO-CLM itself is coupled online to the next smaller COSMO instance. COSMO-CLM (COSMO model in Climate Mode version 5.0) is the community model of the German regional climate research community jointly further developed by the CLM-Community (COSMO-CLM, ROCKEL et al., 2008)

A detailed explanation and schematic overview of the MECO(n) system is provided by KERKWEG and JÖCKEL (2012a) and KERKWEG and JÖCKEL (2012b). Here, we apply the model in a MECO(2) configuration, consisting of one global EMAC instance and two high-resolution COSMO instances CM_40 (40 km) and CM_3 (3 km). The EMAC instance is used as the driving model, i.e. generating initial and boundary conditions, for CM_40, which is the driving model for CM_3 respectively. The domains are depicted in Fig. 2. The (one-way) online coupling between instances is performed at every step of

Table 1: Configuration of the Base models within the MESSy system. For EMAC and both MECO instances CM_40 and CM_3 use the same MESSy configuration.

Submodules	EMAC	CM_40	CM_3	Description	Reference
AEROPT	x			Aerosol optical Properties	(DIETMÜLLER et al., 2016)
AIRSEA	x	x	x	Air sea exchange	(POZZER et al., 2006)
CLOUD	x			Cloud processes	(ROECKNER et al., 2006)
CLOUDOPT	x			Cloud optical properties	(DIETMÜLLER et al. (2016)
CONVECT	x	x		Convection parameterisation	(TOST et al., 2006)
CVTRANS	x	x		Convective tracer transport	(TOST et al., 2010)
DDEP	x	x	x	Dry deposition processes	(KERKWEG and JÖCKEL, 2012a)
E5VDIFF	x			ECHAM vertical Diffusion	
EC2COSMO	x			ECHAM5 fields for COSMO coupling	(KERKWEG and JÖCKEL, 2012a,b)
GMXE	x	x	x	Aerosol Thermodynamics and Microphysics	(PRINGLE et al., 2010)
JVAL	x	x	x	Photolysis rates of chemical tracers	(LANDGRAF and CRUTZEN, 1998)
LNOX	x			Lightning NO _x production	(JÖCKEL et al., 2006)
MECCA	x	x	x	Gas-phase chemistry	(POZZER et al., 2006; SANDER et al., 2011)
MMD	x	x	x	Coupling and multi model driver	(KERKWEG and JÖCKEL (2012b); KERKWEG et al. (2018)
MSBM	x	x	x	Stratospheric multi-phase chemistry	JÖCKEL et al. (2010)
OFFEMIS	x	x	x	Offline emissions of trace gases and aerosols	(KERKWEG and JÖCKEL (2012a)
ONEMIS	x	x	x	Online calculated emissions	(KERKWEG and JÖCKEL (2012a)
ORBIT	x	x	x	Earth Orbit Calculations	(DIETMÜLLER et al., 2016)
OROGW	x			Orographic gravity wave drag	(ROECKNER et al., 2006)
QBO	x			Assimilation of QBO zonal wind observations	
RAD	x			Radiative transfer calculations	(DIETMÜLLER (2016)
SCAV	x	x	x	Scavenging and wet deposition of aerosols and gas phase tracers	(TOST et al. (2006a)
SEDI	x	x	x	Sedimentation of aerosols	(JÖCKEL et al., 2006)
SURFACE	x			Surface properties	(JÖCKEL et al. (2016)
TREXP	x			Tracer release experiment	(JÖCKEL et al. (2010)
TROPOP	x	x	x	Diagnostic calculation of troposphere height	(JÖCKEL et al., 2006)

the driving model. Consequently, a high temporal resolution of boundary conditions for the COSMO/MESSy instances is achieved. Coupling intervals of 12 minutes for CM_40 and 4 min for CM_3, are useful to investigate short term changes, e.g. of short lived chemical tracers, in the MECO domains as it provides a consistent set of boundary conditions.

The EMAC instance is configured to have a truncated T106 horizontal resolution resulting in a gaussian grid spacing of about 1.125°. The vertical discretisation consists of 31 pressure hybrid levels in the ECMWF configuration.

The CM_40 domain consists of a 138 × 128 grid with a horizontal grid spacing of 0.44° and a vertical resolution of 50 pressure levels up to 20 hPa. The vertical resolution increases with height with 13 levels from the ground up to 1000 m, with level mid-points being [10 m, 30 m, 51 m, 94 m, 119 m, 189 m, 249 m, 318 m, 407 m, 517 m, 652 m, 801 m, 965 m] and 10 m being the lowest level. The CM_3 domain consists of 200 × 200 grid cells with a spacing of 0.03° and the same vertical resolution of 50 pressure hybrid levels.

The MESSy configuration of the different instances is presented in Table 1. The selection of submodules and

processes in the EMAC instance is based on the RC1-aero-06 configuration of (JÖCKEL et al., 2016). For the CM_3 instance, the deep convection parameterisation is disabled, assuming the grid spacing of about 3 km is fine enough to resolve convection related processes reasonably well.

Anthropogenic emissions are prescribed by monthly mean values. For EMAC and CM_40 we apply the 50 km MACCity emissions (LAMARQUE et al., 2010) from the RCP8.5 scenario for the year 2010. For the CM_3 domain 7 × 7 km TNO-MACCIII emissions (KUENEN et al., 2014) for the year 2011–2014 are used. In order to account for temporal characteristics of emissions, time profiles are applied using MACC-II hourly emission factors for traffic emissions in the CM_3 domain.

The selected gas phase mechanism, mim1-CCMI-base2, considers the basic reaction cycles of ozone, methane and odd nitrogen as well as alkanes and alkenes up to C₄. For the chemistry of isoprene the Mainz Isoprene Mechanism (MIM1) (PÖSCHL et al., 2000) is added. For a comprehensive description of the mechanism we refer to (JÖCKEL et al., 2006) and its electronic supplement.

2.3 Functionality and configuration of TERRA_URB

The urban canopy parametrization within MECO(n) is achieved via the urban-canopy land-surface scheme TERRA_URB (SCHULZ et al., 2016; WOUTERS et al., 2016b) which basically includes urban physics in the COSMO(-CLM) model (STEPPELER et al., 2003; ROECKNER et al., 2006) by modifying the surface module TERRA-ML (SCHULZ et al., 2016; SCHULZ and VOGEL, 2020) and the corresponding land atmosphere interactions. TERRA_URB consists of the bulk representation of the urban canopy (DEMUZERE et al., 2008; DE RIDDER et al., 2012). The original version of CCLM in MECO(n) has a standard representation of urban land by modifying soil and vegetation parameters in the Soil-Vegetation-Atmosphere Transfer model TERRA (DOMS, 2011). It does however not resolve specific urban features, such as shadowing effects or thermal and radiative properties of building materials and street canyons. While sub-grid scale surface heterogeneity was originally ignored in TERRA_ML, a poor man’s tile approach is applied within TERRA_URB, allowing urban and natural tiles to co-exist within one grid cell. Total grid-cell fluxes from the surface into the boundary layer thus represent an average from urban and natural land according to their respective fraction. The percentage of impervious surface area in one grid cell is calculated from a 10’’ data-set for Europe (MAUCHA et al., 2010). The variation of natural land in the remaining natural tiles is controlled over the variables PLCMN (minimum plant cover) and PLCMX (maximum plant cover).

The urban morphology is defined via building area fraction (BF), mean building height (H) and height-to-width ratio (H/W). The latter is used to calculate the sky view factor. The urban scheme hence provides corrections of the surface parameters within TERRA and integrates road, roof and wall surfaces into a 2D horizontal surface for which radiative and thermodynamic properties are adapted according to the 3D structure of the urban canopy. This is done through the semi-empirical urban canopy dependency parametrization SURY (WOUTERS et al., 2016a), while the three-dimensional urban canopy information is translated via bulk parameters following WOUTERS et al. (2016a) and TRUSILOVA et al. (2016). Default central Europe specific urban canopy parameters are defined as input for SURY according to LORIDAN and GRIMMOND (2012) and given as output to TERRA_URB (Table A.1).

The surface layer transfer coefficients for momentum and heat are determined in a non-iterative way (WOUTERS et al., 2012). Urban land cover has a specific thermal inertia (DEMUZERE et al., 2008), roughness length, albedo and emissivity (SARKAR and RIDDER, 2011; WOUTERS et al., 2013; DEMUZERE et al., 2017) and accounts for surface layer stability and the roughness sub-layer. Besides that, it considers a non-iterative surface layer flux $kB^{-1} = \ln(z_0/z_{0h})$ parametrization in the surface-layer transfer scheme for the urban fab-

Table 2: Overview of the experiments/scenarios performed in this analysis.

Experiment	Model	Comment
BASE	CM_3	Reference Simulation with the full TERRA_URB parameterisation
NO_URB		without special URB parametrisation, only TERRA
ISA_plus		increased ISA in urban areas representing a densification of urban areas
ISA_minus		decreased ISA in city centers and increased ISA in the surroundings

ric with z_0 and z_{0h} being the aerodynamic and thermal roughness lengths. This ‘Bluff-body’ thermal roughness length parameterisation follows the approaches given in BRUTSAERT (1982), KANDA et al. (2007) and DEMUZERE et al. (2008). A new bare soil evaporation resistance formulation (SCHULZ et al., 2015) is included next to the vegetation skin temperature parametrization of SCHULZ et al. (2015) and VITERBO and BELJAARS (1995). In our study we take parameters for albedo, emissivity, heat capacity and heat conductivity and aerodynamic roughness length following WOUTERS et al. (2015b) and WOUTERS et al. (2016a). Other than in NO_URB, evaporation from urban surfaces is taken into account and impervious water storage is based on a density distribution of water puddles (WOUTERS et al., 2015a). TERRA_URB has already been tested both offline and online for many cities around the world (WOUTERS et al., 2015b; WOUTERS et al., 2016b; DEMUZERE et al., 2017) including Toulouse, Basel, Singapore, Vienna, Turin, and urban areas in Belgium.

2.4 Experiments and simulations

By switching on the option `lterra=.True.`, various urban specific parametrizations are considered and activated in TERRA-ML, modifying (near-) surface temperature values, surface variables and heat fluxes. Consequently, the UCM reduces the grid cell latent heat flux and increases the sensible part with respect to its impervious fraction, which is particularly true at nighttime (compare Fig. 5). Assessing the impact of TERRA_URB on MECO(n)-output variables, an urban setup (BASE) can be compared to a non-urban configuration (NO_URB) with `lterra=.False.` By modifying various surface parameters within SURY, sensitivity tests can be performed representing dedicated urban planning scenarios. In this study, the experiments ISA_plus (densification) and ISA_minus (urban sprawl), which are both variations of BASE, are compared. More details are given in Chapter 3.4. Table 2 presents an overview of the performed simulations

3 Results and discussion

In order to assess the functionality and evaluate the added value of the urban canopy model TERRA_URB

Table 3: Evaluation for station Mainz-Mombach (OBS) for grid cell value (marked black in Fig. 3b) of the simulation including TERRA_URB (BASE) and TERRA_URB switched off (NO_URB) showing absolute values and biases averaged over the model period July 1–10 2018. Bold values indicate the lowest bias of the respective setup BASE or NO_URB.

	2 m temperature [°C]		10 m windspeed [ms ⁻²]		10 m wind direction [deg]		2 m relative humidity [%]		surface ozone [ppb]		surface NO _x [ppb]	
	day	night	day	night	day	night	day	night	day	night	day	night
BASE	23.80	17.10	2.94	2.08	181	134	43.60	61.02	51.20	38.60	7.18	10.57
NO_URB	22.90	16.50	2.98	2.11	183	126	47.69	64.58	50.40	36.80	8.00	11.10
OBS	25.05	17.69	2.05	1.20	200	200	39.21	56.31	46.97	41.81	8.71	10.11
BASE_bias	-1.25	-0.59	0.89	0.87	-24	-66	4.39	4.70	4.23	-3.21	-1.53	0.46
NO_URB_bias	-2.15	-1.19	0.93	0.90	-22	-74	8.49	8.27	3.43	-5.01	-0.91	0.99

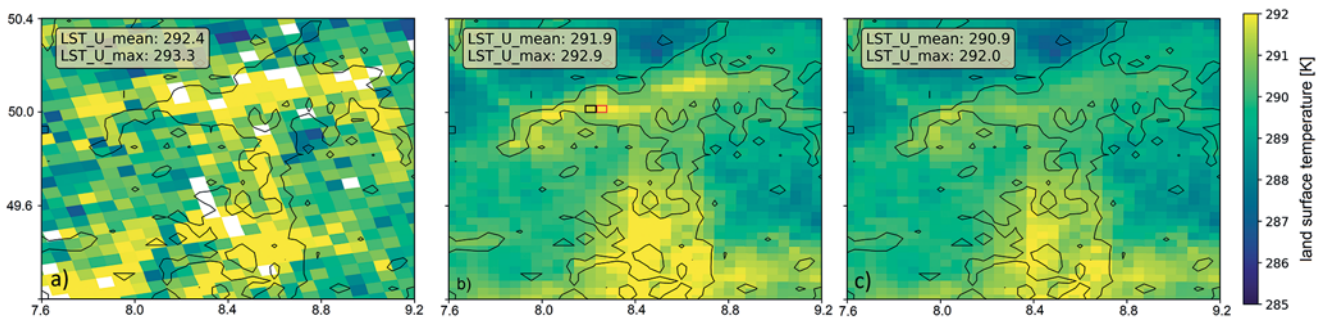


Figure 3: Land surface temperature (LST) retrieved from MODIS TERRA for 1 July 2018 21:15 UTC (a) and equivalent model time step for BASE (b) and NO_URB (c). Note the red and black boxes in (b) indicating the locations of measurement stations for further analysis.

for meteorological and air chemical simulations with MECO(n), we compare surface, air temperature and NO₂ observations, with air temperature being analysed over the boundary layer as well. Other variables such as wind speed, wind direction, relative humidity and ozone are analysed statistically (Table 3).

3.1 Evaluation of surface temperature

The land surface temperature (LST) product from MODIS-TERRA is retrieved from the catalogue of satellite products (earthexplorer.gov) and resampled to the model resolution of 3 km (Fig. 3a). Being 95 % cloud free, we select 1 July 2018 21:15 UTC and extracted the region around the Rhine-Main metropolitan area (contour in Fig. 3). White areas in Fig. 3a display cloud pixels. According to observation, the maximum difference between the temperature of an urban (inside contours) and a rural grid cell (outside contours) amounts to 7.7 K. The contour line encloses an area with an impervious fraction higher than 30 %. The mean urban land surface temperature (LST_U) inside that line accounts for 292.4 K. Maximum recorded temperature amounts to 293.3 K respectively. In comparison, model output from the BASE run underestimates maximum LST_U by 0.5 K and mean LST_U by 0.4 K (Fig. 3b). With 1.5 K and 1.3 K, the underestimation however is significantly increased when switching off the urban canopy model in NO_URB (Fig. 3c). For this specific date and

time, we expect the coupled simulation BASE improving the representation of the surface urban heat island compared to the uncoupled NO_URB run.

3.2 Evaluation of temperature and NO₂

Urban background stations for 6 selected medium sized urban areas inside CM₃ (green circles in Fig. 2) have been compared for 2 m air temperature (Fig. 4a). Further statistics have been calculated with regard to wind speed, wind direction, relative humidity, ozone and nitrogen oxides (Table 3) at the urban background measurement location Mainz-Mombach (blue box in Fig. 3b).

The model in general underestimates 2 m air temperature, with the mean bias averaged over 10 days and 6 urban (Table A.2) background stations with 0.8 K for BASE and with 1.6 K for NO_URB respectively. Due to slight shifts in timing, some values in the box plot (Fig. 4a) reach -4/+4 K but can be seen as outliers. Although the night-time mean bias for NO₂ is slightly increased for BASE compared to NO_URB (see also Table 3), the 95 percentiles of NO₂ concentration (dots in Fig. 4b) are more correctly represented at least for some areas by the simulation including TERRA_URB. For the single station Mainz-Mombach, the relative bias in peak concentration is decreased from 0.25 (NO_URB) to 0.18 (BASE).

Analysing four meteorological variables, i.e., 2 m air temperature, 10 m wind speed, wind direction and

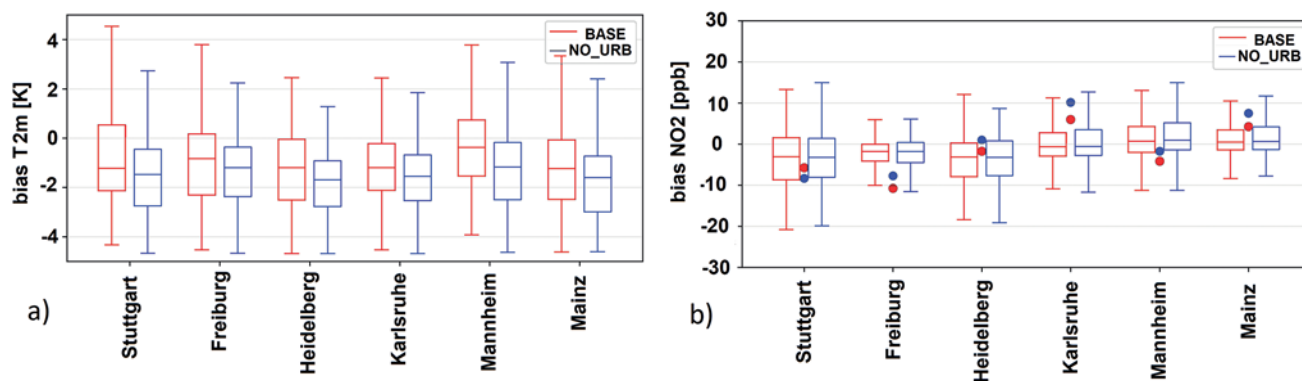


Figure 4: Hourly 2 m air temperature for 1–10 July 2018 for 6 selected urban background stations (Table A.2) (a) and hourly surface NO₂ concentration with dots representing 95 interval of maximum concentrations (b) comparing the BASE (red) and the NO_URB experiment (blue).

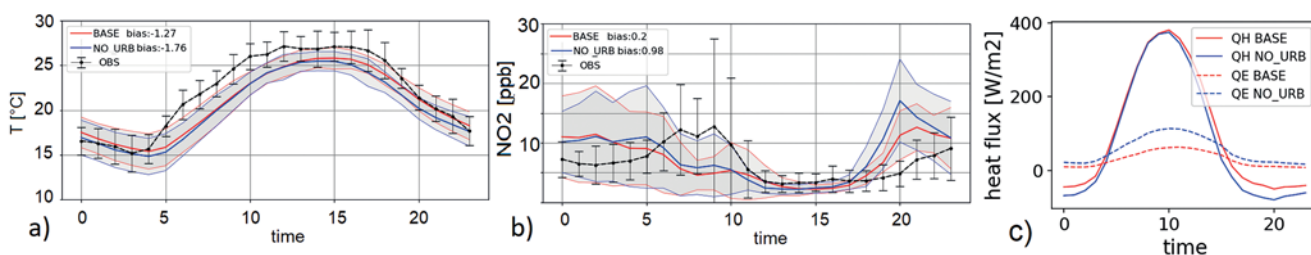


Figure 5: Mean diurnal cycle averaged over the model period 1–10 July 2018 for station Mainz-Mombach and respective grid cell (marked black in Fig. 3b) for 2 m temperature [°C] (a) and NO₂ [ppb] (b), with red color being BASE and blue color NO_URB. Dashed black lines represent observations at Mainz-Mombach. Error bars and grey shading show hourly standard deviation over 10 days for OBS and model respectively. Diurnal mean sensible (solid) and latent (dashed) heat flux [W/m²] shown in (c).

2 m relative humidity, averaged over 1–10 July 2018 for day (0700–2100) and night (2100–0700) we find mean biases improved for both periods for all variables except for wind direction (bold letters in Table 3). For secondary pollutants NO_x and ozone, we find lower biases for the NO_URB configuration during the day, with the latter most likely to be explained by lower NO_x biases as both pollutants are chemically linked. Due to the coarse resolution of the model grid and the emission data set, only urban background stations are adequate for model-observation comparison in an urban context. With the measurement station Mainz-Mombach, officially classified as an urban background station we evaluate the model comparing hourly mean values averaged over 10 days model time. For the comparison, we use the grid cell that has the closest distance to the geographical location of the measurement point. Hence, the model is not able to capture the local flow conditions at the exact measurement location but rather represents a background meteorology. With absolute differences between day and night being in the same order, simulated diurnal averages are about two times higher than observed ones. Wind speed is generally very low at that location and time.

In order to get a more detailed picture on the diurnal cycle of temperature and NO₂, diurnal mean values are calculated from the model output for the urban

background station Mainz-Mombach. With a decrease of the mean bias in 2 m temperature (Fig. 5a) averaged over the model period 1–10 July from -1.27 (BASE) to -1.76 K (NO_URB), most of the bias reduction can be accounted to night-time and late evening where the diurnal profile of BASE is shifted closer towards the observed value. Single Buildings are not represented but parameterized within TERRA_URB. Following MUSSETTI et al. (2020), it is hypothesized that heat storage in building materials and increased trapping of longwave radiation in street canyons and release of surface sensible heat at the ground and from the building surfaces acts as heat source for the lowest model layer both at day and night-time. The introduction of building effects in BASE considers a sky view factor, which hampers radiative cooling at night-time. In combination with the reduced evaporative cooling, an increase of roughness length from 4.8 m (NO_URB) to 6.1 (BASE), heat storage in building walls and roofs and an anthropogenic heat flux, a central urban grid cell in BASE shows decreased latent heat flux and a reduced sensible heat loss at evening and night-time compared to NO_URB (Fig. 5c). With an impervious surface area fraction of 0.48, the respective grid cell is considered as suburb-like, with still a significant amount of natural vegetation. The temperature bias reduction is in the same order as reported for the urban area of Berlin by TRUSILOVA et al. (2016).

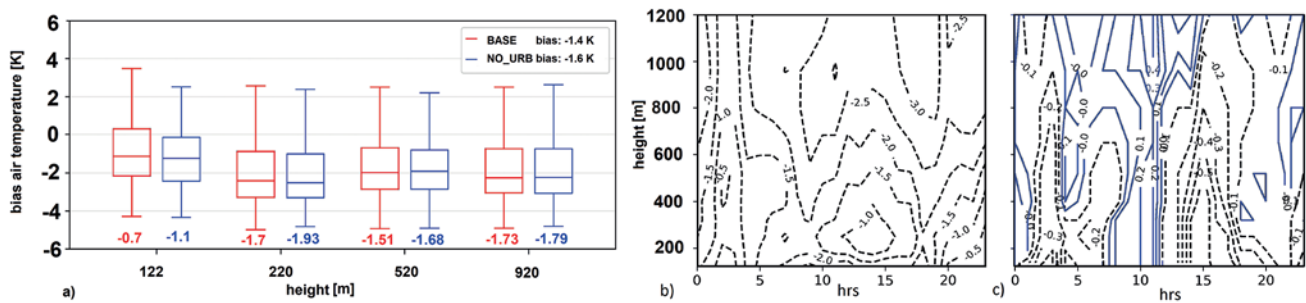


Figure 6: Boxplots of temperature biases BASE-OBS_RAD (red) and NO_URB-OBS_RAD (blue) (red colour rectangle in Fig. 3b) observed temperature for four different heights (a) as well as hovmoller time-height plots showing biases BASE-OBS_RAD (dashed) (b) and the difference of the two model biases (BASE-OBS_RAD)–(NO_URB-OBS_RAD) (c). Negative values indicate a bias reduction (dashed) when using TERRA_URB, positive values an increase (blue).

In addition, we find a simultaneous bias reduction of NO_2 from 0.98 to 0.2 ppb, accounting for a relative bias reduction from 0.31 to 0.23 (Fig. 5b). While both configurations BASE and NO_URB fail to capture the diurnal cycle, especially with regard to the morning peak, the evening and night-time reduction leads to an average improvement of the representation of an urban background location. It has to be noted, that a model with coarse resolution is hardly able to account for small-scale features and can not necessarily be used for local air quality assessment. The selection of the measurement station is another point that has to be addressed critically. The comparison with a central urban station showed a large underestimation as local sources were not accounted for. Therefore, the only valid station in the area of interest was Mainz-Mombach, which is officially classified as ‘urban background’, and best represents background air quality in that area. Hence, the prevailing local conditions at the station were not considered.

The impact of the UCM throughout the urban boundary layer is assessed comparing vertical temperature information for the model levels with ground based remote sensing data (OBS_RAD) retrieved from the passive micro wave radiometer from the Environmental Agency at roof level (30 m) (location marked red in Fig. 3b). Due to the technical functionality, values below 120 m height are not recorded in the radiometer measurement. Fig. 6a shows box plots for a model period of 10 days evaluated for four different heights within the urban boundary layer. Averaged over the entire column (represented by these four heights) we find a mean bias of -1.4 K for BASE and -1.63 K for NO_URB respectively. The highest difference in model bias exists for the lowest height (122 m), while the impact of the urban canopy model on the thermal properties of the urban boundary layer decreases with height confirmed by decreasing differences in the biases between BASE and NO_URB (Fig. 6a). In the course of the day, we find the highest underestimations of the BASE run during daytime with values from -1 K (120 m to 400 m) to -2.5 K (>800 m). The night-time bias is lower from 120 m to 800 m (Fig. 6b). Fig. 6c shows the differences

between both biases [BASE-OBS_RAD]–[NO_URB-OBS_RAD], with negative values indicating a lower bias on the side of BASE. Following the diurnal evolution of the boundary layer, the largest impact of the urban canopy and TERRA_URB respectively on the thermal structure of the urban boundary layer is noticed around 15:00 hrs with -0.7 K up to approximately 400 m to about -0.2 around 1000 m. At evening and night-time, that bias is reduced to -0.3 to -0.1 for the heights 200 to 400 m respectively. From Fig. 6b,c it can be concluded, that the impact of the urban layer on the overlying atmosphere reaches up to about 1000 m in the afternoon and between 200 to 600 m in the evening and night-time. These results are well in line with findings for Berlin (GEISS et al., 2017) or for Budapest (EMEIS and SCHÄFER, 2006). It has to be noted however, that the quality of the radiometer observations is not assessed.

The findings from this section are well consistent with other studies. In terms of NO_x , (SARRAT et al., 2006) using the MESONH atmospheric model (LAFORE et al., 1997) coupled with the urban canopy model TEB, shows that during night-time, the surface NO_x and ozone concentrations over Paris are better reproduced when an urban scheme is used. This is because the boundary layer stays near neutral over the city, and is relatively deep (MASSON, 2006; DEMUZERE et al., 2017).

3.3 Sensitivity of urban canopy parametrization to imperviousness

Difference plots between BASE and NO_URB for the predefined area (urban agglomeration Mainz, Frankfurt, Mannheim) of the model domain show the impact of the urban canopy parametrization on the surface temperature, air temperature and NO_2 concentration. With central urban grid cells ($\text{ISA}>0.4$) sticking out particularly at daytime with regard to surface temperature (7b), the largest feedback of building structures on air temperatures can be found for night-time periods 2100–0600 UTC. Stored in building materials during the day, energy is released into a stably stratified night-time urban boundary layer, followed by local heating of urban air within the respective grid cells (Fig. 7f). Due

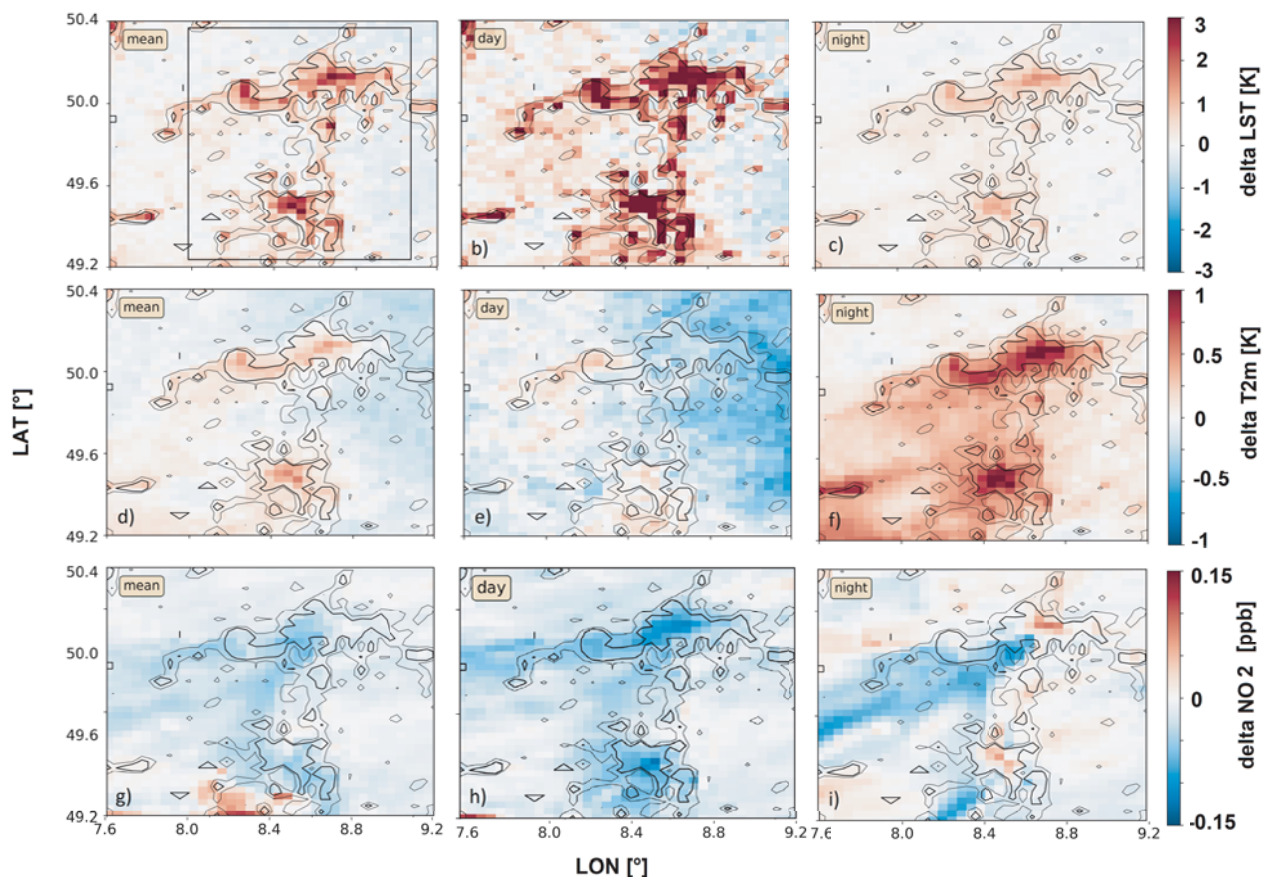


Figure 7: Mean bias BASE-NO_URB extracted for CM_3 for the Rhine-Main urban area and surrounding for surface temperature (LST) (a–c), 2 m air temperature (T2m) (d–f) and NO₂ (ppb) (g–i). Means over the model period 1–10 July 2018 (a,d,g), the daytime (07–21 UTC) in b, e, h and night-time (22–06 UTC) in c, f, i. Bold black contour lines indicate central urban area (threshold ISA>=0.3) and light contour urban background (0.1>ISA>0.3). Black box in 7a represents urban area discussed in Fig. 9.

to weak mean wind, the effect on 2 m air temperature is locally limited to the urban grid cells, correlating to the spatial patterns of surface temperature change in 7b. Maximum difference between urban and rural surface temperature – namely surface urban heat island amounts to 6.3 K at around 1400 UTC and to 2.1 K with respect to the canopy UHI, represented by 2 m air temperature at 2200 UTC. Both values are calculated from the mean over the model period. Maximum grid cell urban canopy effects account for 4.8 K (surface temperature) and 1.7 K (air temperature), respectively. Near surface NO₂ concentrations, during the day are reduced by a factor of –0.20 (–20 %).

The impact of TERRA_URB coupling on model variables for various degree of surface sealing is tested on the basis of the correlation between impervious surface area and change in thermal or chemical state of the lower urban boundary layer, represented by surface and air temperature (absolute) and NO₂ (fractional reduction), respectively.

All grid cells in the model domain over a predefined threshold of ISA>0.1 (10 % impervious) are grouped into 30 classes with 2 % intervals. The size of the respective scatter indicates the number of members within

each interval. For each grid cell, the difference between BASE and NO_URB is calculated and averaged over the respective class cluster. With respect to Fig. 8a,b we find a positive correlation between imperviousness and temperature change, with the impact of TERRA_URB increasing with increasing ISA. The impact on NO₂ near the surface in Fig. 8c is anti-correlated to ISA, indicating the effect of more intense vertical mixing due to increased vertical fluxes from surfaces with higher temperature (Fig. 8a). As indicator for increased vertical fluxes, we added the difference in z-wind component over the boundary layer in Fig. 9a. It becomes obvious from Fig. 8a,b that higher absolute differences are to be expected for daytime with regard to surface- and for night-time for air temperature. NO₂ concentrations are presented for daytime (time with highest emissions) only as no correlation is to be found for night-time (Fig. 8c). Aiming for a more detailed analysis of the inter-dependencies between surface NO₂ concentration and both ISA and NO_x emission flux we zoom into the Rhine-Main urban area (Fig. 8d–e).

In the three city clusters (8d,e) Frankfurt (F), Mainz (Mz) and Mannheim/Ludwigshafen (Ma) with dots representing grid cells with an impervious fraction >0.4,

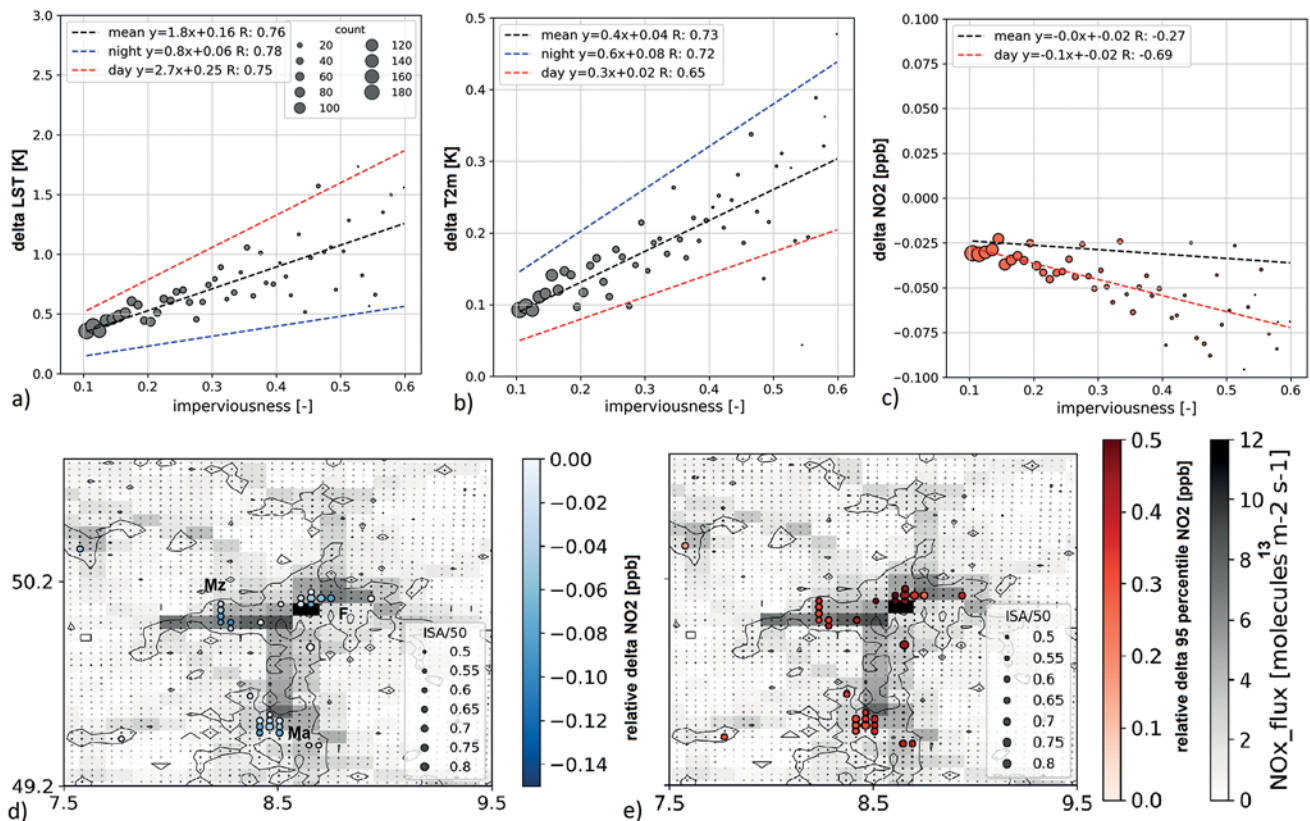


Figure 8: Correlation between impervious surface (ISA>0.1) and model biases BASE-NO_URB for surface temperature (a) 2 m air temperature (b) and NO₂ (c) at the respective urban grid cells. Scatter plots presented for mean values over 1–10 July 2018, sizes of dots represent the number of grid cells within one class of bin width 0.01. Regression lines for daytime mean (07–21 UTC) in red and for night-time (22–06 UTC) in blue. A zoom to the Rhine-Main urban area is shown in Fig. 8d,e with underlying NO_x MACCIII emissions in gray and blue shaded dots presenting the mean bias BASE-NO_URB. Sizes indicate the impervious surface fraction (d) and red shaded dots showing the mean bias only considering the upper 95 percentile of NO₂ concentration representing the daytime emission peaks (e). Location of scatter in (d, e) indicate three city clusters Mainz (Mz), Frankfurt (F) and Mannheim (Ma)

daily mean NO₂ near-surface concentration is decreased by -0.15 (-15%) (8d). The largest relative impact however is not concentrated in the area with highest emission fluxes, but for grid cells with highest impervious fraction. While mean values sometimes mask short time, localised effects, the 95th percentile of the simulated NO₂ concentrations, coinciding with the daytime traffic peaks shows a temporary increase of surface NO₂ concentration (8e). This can be explained by the emission of NO_x into a changed urban morphology within TERRA_URB, represented by mean roof heights and building widths. Again, the highest relative increase of up to 0.5 ($+50\%$) is to be found at grid cells with highest impervious fraction. Hypothetically, two additional effects happen here, next to mechanical shear introduced by roughness elements. Firstly, increased heating rates in the morning hours slow down, affecting internal boundary layer growth and more pollutants accumulate in the internal boundary layer, before it penetrates the residual boundary layer aloft. Secondly, weak wind conditions lead to the fact, that residual heat and pollutants present in the upper layers mix down. Detecting these small convergences within the urban boundary however is hard to detect at a model resolution of 3 km.

In Summary that means, that the way, the urban canopy is represented in the model, governs the dynamical exchange in the urban boundary layer. In average, using TERRA_URB results in a relative decrease of NO₂. During morning and evening traffic peaks however, the changed urban morphology from NO_URB to BASE results in a temporary blocking and relative increase of NO₂.

Hovmoller difference plots for temperature and NO₂ (Fig. 9) and the vertical profile for the vertical wind component (blue line in 9a) indicate that surface warming (Fig. 7) triggers enhanced vertical mixing over the urbanized region (box in Fig. 7a). Unless in reality fluctuations of the ascending and descending tendencies vary significantly between different time steps, the average over the model period showed a clear tendency. Pollutants emitted during daytime, are consequently distributed to higher levels (9b). Hence near surface NO₂ levels are decreased by -0.2 . With -0.15 (-15%) reduction, the modifications in surface energy balance are still noticeable at about 300 m height (Fig. 9b). The vertical transport of pollutants from the ground to higher levels above the urban canopy is indicated by an NO₂ surplus aloft. Warming plumes emerge in

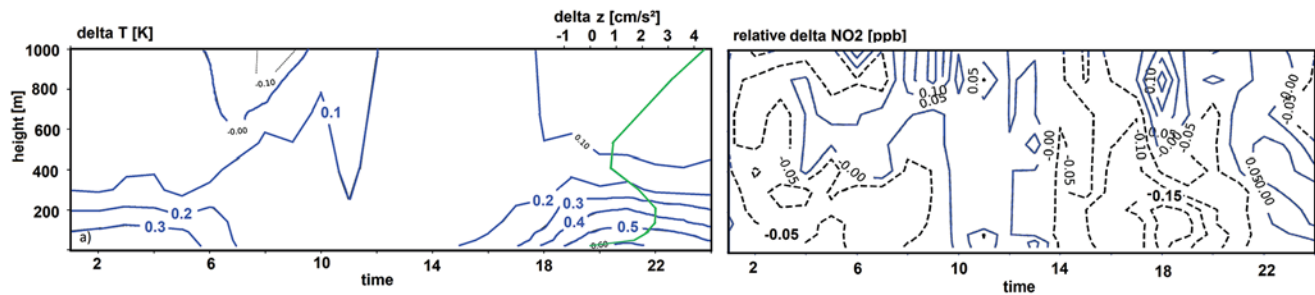


Figure 9: Hovmoller diagrams for air temperature [K] absolute (a) and NO_2 concentration [fraction] relative difference (b) of BASE- NO_URB averaged over the urban area of Mainz/Frankfurt as indicated by bold contour ($\text{ISA} \geq 0.3$) in Fig. 7 presented as hourly means over the model period 1–10 July 2018. Blue contour indicate an increase, dashed lines a decreasing trend. Green line indicate a profile of the difference in z-wind component averaged of all days at 2000 hrs.

the BASE simulation, only due to the representation of the urban canopy by TERRA_URB in the time between 1700–0700 UTC (Fig. 9a). They lead to a surplus of 0.1–0.4 K and a decrease in NO_2 levels of up to -0.30 (-30 %).

A slightly reversed tendency occurs between 0800 and 1200 hrs, with a relative increase reaching up to +5 %. Here, denser building structures introduced by the UCM lead to trapping of NO_2 originating from morning emissions.

These kinds of model systems are hardly capable of capturing short time and localized effects. In order to draw general conclusions on the interplay between urban morphology, dynamics and air chemistry, we focussed on mean values only, unless they might not be adequate for snapshots. In terms of relative reductions, we only look at the differences between the two model runs BASE und NO_URB , neglecting the results from the evaluation and the problems of the model to properly represent the observed diurnal cycle.

3.4 Case Study – Sensitivity of building density on urban heat and air quality

The existing model configuration allows for case study experiments considering various strategies how urban areas in Germany can be planned taking the projected expansion of urban space (UMWELTBUNDESAMT, 2019) into account. Urban population in Germany is estimated to increase from 76.4 % (2018) to 78.6 % in 2030 (UNITED NATIONS, 2018). In this chapter, we analyse two scenarios of urban development, a re-densification of the urban centre or a push towards the close vicinity, representing an urban sprawl. This scenario necessarily has to happen at the cost of natural land near the urban areas. Both experiments are controlled via the variables ‘ISA’ and ‘URBAN’, representing the fraction of impervious surface and the fraction of urban classified area in a 3×3 km grid cell (2b). For highly impervious urban grid cells ($\text{ISA} > 0.4$), ISA_plus considers an increase of impervious surface area fraction per grid cell by 50 % (10a, bottom), which is equivalent to a 50 % decrease of natural land cover in the same cell. ISA_minus considers

a decentralization of urban space with an increase in the closest rural surrounding at the simultaneous decrease in the urban centres. The experiment is realized, decreasing the impervious fraction in the core urban grid cells by 30 % and increasing the impervious fraction by 80 % for the grid cells in close vicinity where ISA is in the range of [0.1,0.3] in the BASE simulation (10a, top).

The extracted area of interest (10a) consists of 289 grid cells with 43 accounting for an impervious surface area fraction $\text{ISA} > 0.3$. The highest value in that area according to the ISA-dataset (MAUCH, G., G. BÜTTNER and B. KOSZTRA, 2010) amounts to 0.78. Fig. 10 analyses the scenarios’ (ISA_minus , ISA_plus) impact on surface temperature (10b) and air temperature (10c) and urban heat island with respect to the areas depicted in Fig. 10a averaged over grid cells with an impervious surface area fraction of $\text{ISA} > 0.4$. The urban heat island for surface and air temperature is calculated as difference between the mean over all urban grid cells with $\text{ISA} > 0.4$ and the mean of all rural cells with $\text{ISA} < 0.01$. The difference to the default configuration (BASE) indicates the impact of the respective scenario.

Surface temperature averaged over the central urban area with $\text{ISA} [0.4, 1.0]$ shows a maximum increase during the daytime of about 4 K at 1400 hrs for ISA_plus , when incoming solar radiation peaks and building materials, roads and other sealed surfaces accumulate the energy surplus and consequently heat up (Fig. 10b, left, red shading). The difference between ISA_minus – and BASE shows a minimum (although about 1–2 hours earlier), as a higher percentage of natural tiles moderate surface warming. Contrasting the two scenarios, the maximum surface urban heat island increases in ISA_plus to about 9 °C, while it decreases in ISA_minus to 3 °C compared to BASE showing an UHI of up to 6.3 K. The diurnal cycle of the urban heat island follows the observed change in temperature difference, resulting from the increase of impervious surface area in the centre. On average, an increase of surface temperature of about 3 K during the day, leads to a 0.5 K increase in air temperature aloft, during night-time. At solar noon, a major part of the incoming energy is stored in the building materials. That can explain the slight decrease during the day

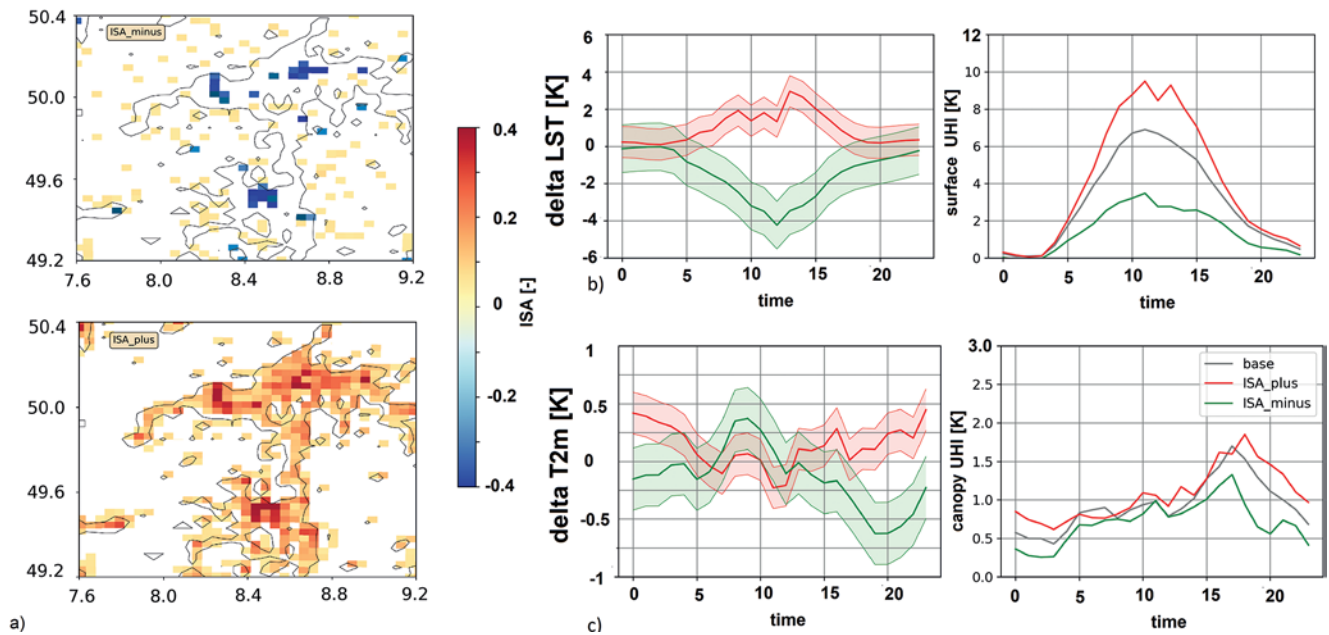


Figure 10: Change in impervious surface area presented as difference ISA_minus-BASE, ISA_plus-BASE (a) extracted for the Rhine-Main urban area and mean difference in surface temperature (delta LST) and surface urban heat island (b) and 2 m air temperature and canopy heat island (c) with delta ISA_plus-BASE (red), delta ISA_minus-BASE (green) and BASE (gray). For UHI calculation, urban area covers all grid cell within box in Fig. 7a with the criterion ISA[0.4,1.0] and rural grid cells include all grid cells with ISA[0,0.01] in the same box.

(Fig. 10c, left, red). These results are in line with recent findings from satellite observations for the urban area of Boston (CHANG et al., 2021).

Air temperature in urban grid cells with tiles largely converted from urban to natural (vegetation) slightly increases in the morning compared to BASE, as broader urban canyons allow the flat-angle incoming radiation to enter the urban canopy and warm the surrounding air masses. Shadowing effects in the model are considered via the sky view factor, which is calculated by the relation between building height and road width. Reducing the imperviousness in ISA_minus considers a higher percentage of natural, open space per grid cell and a reduced contribution of the sky view factor to the overall grid cell mean value. In the evening and night-time, evaporative cooling of natural tiles comes into play and lead to relative cooling of urban air. Differences with regard to canopy urban heat island (Fig. 10c – right) are most pronounced during evening and night-time for ISA_plus increasing by about 0.4 K. ISA_minus simulates a maximum decrease of -0.6 K around 2000 UTC. Between 2000 to 2200 UTC the gradient is reversed (Fig. 10c right, green) as grid cells in the rural surrounding with a relative increase in impervious surface fraction due to urban sprawl effects (10a, top) hampering the evaporative cooling performance of neighbouring rural grid cells. Except between 1200 and 1300 UTC, the canopy UHI (calculated from 2 m air temperature) is decreased for ISA_minus for the entire model period. The increase in ISA_plus is limited to evening, night-time and noon. Surface temperature averaged over model period and core urban area is increased by 1.1 K for ISA_plus and decreased by 1.5 Kelvin for ISA_minus

compared to BASE. This translates to an average increase of 2 m air temperature of 0.2 K in a densified built-up environment and a decrease of 0.3 K for a greener, more open canopy. While surface temperature urban heat island is increased from 3.1 to 4.1 K for ISA_plus, a decrease from 3.1 to 1.5 is simulated for ISA_minus. Air temperature urban heat island is projected to increase from 0.9 to 1.1 for ISA_plus and decrease from 0.9 to 0.7 for ISA_minus respectively. Technically, the UHI intensity is retrieved from the difference between mean grid cell value for areas with ISA[0.4;0.1] and rural areas with ISA[0;0.1].

Varying the impervious surface fraction for ISA_plus we can assess the sensitivity of temperature change on change in imperviousness (Fig. 11). First, the change of imperviousness from ISA_plus to BASE is calculated per grid cell. These absolute differences are then grouped according to their membership in one of 80 classes of 0.01 width. Sizes of points indicate the number of grid cells in the respective group. The difference in impervious fraction is correlated to the difference in surface temperature (Fig. 11a) and air temperature (Fig. 11b) in the respective group. All grid cells with difference in impervious surface area higher than 0.395 are grouped in the last class accounting for 10 grid cells out of 768 in total. These calculations are done for the Rhine-Main area as depicted in Fig. 7.

Fig. 11a shows a linear correlation between change in imperviousness through densification and change in surface temperature (LST) of $R=0.73$, with a projected temperature increase of about of 0.17 K per 10 % increase in imperviousness. With $R=0.81$, the highest sensitivity of surface temperature towards surface mod-

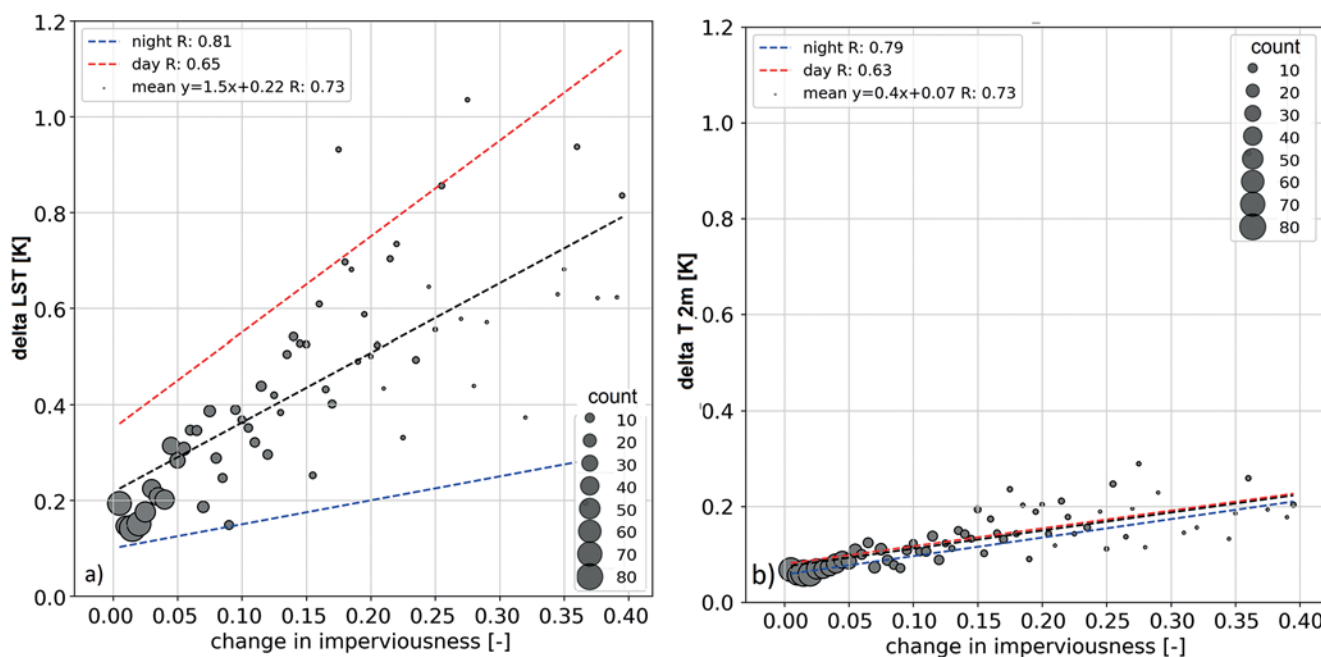


Figure 11: Sensitivity of surface (LST) (a) and air temperature (T2 m) change (b) towards change of impervious surface area fraction for the urban area (bold contour in Fig. 8) when applying the scenario ISA_PLUS. Change in temperature shown for average over model period 1–10 July 2018 (black), daytime (red) and night-time (blue). Sizes of dots indicating the number of grid cells lying within ISA class of 0.01 width.

ification is found at night-time ($R=0.81$), however with a less steep slope. Obtaining an R-value of 0.59, the daytime increase amounts to about 0.2 K per 10 % increase respectively. On the other hand, with regard to air temperature the increase is less than about 0.05 K per 10 % for all times of the day. From Fig. 11 it can be hypothesized that the urban air warms at a maximum rate of 0.2 K per 0.8 K increase in surface temperature. Fig. 11 underlines findings from (MARTILLI et al., 2020) regarding the use of the term ‘urban heat island’ for assessing heat mitigation potentials for climate sensitive urban planning strategies such as urban greening. In their study, they suggest using urban heat levels instead, in particular when considering air temperatures. In the appendix Figure A.1 we have therefore included findings from our simulation which confirm (MARTILLI et al., 2020) with regard to a more detailed analysis of 10 urban regions (boxes in Fig. 2).

Averaged over all urban grid cells with $ISA>0.4$ (as defined in the BASE simulation) and model period, dynamical effects in the urban boundary layer force the relative decrease (red) and increase (green) in near surface (10 m) NO_2 levels for both scenarios (Fig. 12). Being more or less in the same order ($\pm 20\%$ maximum change), the largest impact focusses on the time of the second emission peak from about 1500 to 2000 UTC. Where air pollutants are released into a warmer (ISA_plus) or colder (ISA_minus) and less dynamic urban air – relative to BASE.

The blue line in Fig. 12 indicates the diurnal mean difference in z-wind component in the urban canopy layer (15 m), for the scenario ISA_plus. Positive val-

ues represent an upward directed motion inside a denser and warmer urban environment. That aspect causes the dilution of NO_2 via vertical turbulence. Z-wind differences for ISA_minus are pointing in the opposite direction (not shown).

During evening and night-time however, vertical profiles averaged over the core urban area (bold contour in Fig. 7a) show a relative increase in near surface NO_2 concentrations between 21:00–22:00 hrs by about 10 % for the difference ISA_plus – BASE (Fig. 12b). With the impact of vertical mixing indicated by the blue line in Fig. 12a diminishing in the evening, the blocking feature of a denser urban canopy in ISA_plus compared to BASE comes into play, leading to a relative increase of NO_2 at the surface by about 10 %. This increase is highest at the surface and noticeable up to about 120 m.

Assessing urban air quality necessarily needs to involve other pollutants as well. Tropospheric ozone at high concentrations near the surface for instance is a danger to human health particularly at daytime during heat wave episodes. Model results indicate that overall ozone concentrations are particularly high during the case study period. In denser urban canopies within ISA_plus, elevated near surface levels are simulated, due to excess heat and decreasing NO_2 concentration. That aspect however is only valid for the evening time, when ozone levels already drop. With a mean relative decrease of surface urban NO_2 concentration of about 15–20 %, ozone levels increase by about 4–5 % in average. Similar numbers have been found by other studies looking at covid19 NO_x emission reduction (e.g. Amouei TORKMAHALLEH et al., 2021; MERTENS et al., 2021) A more in

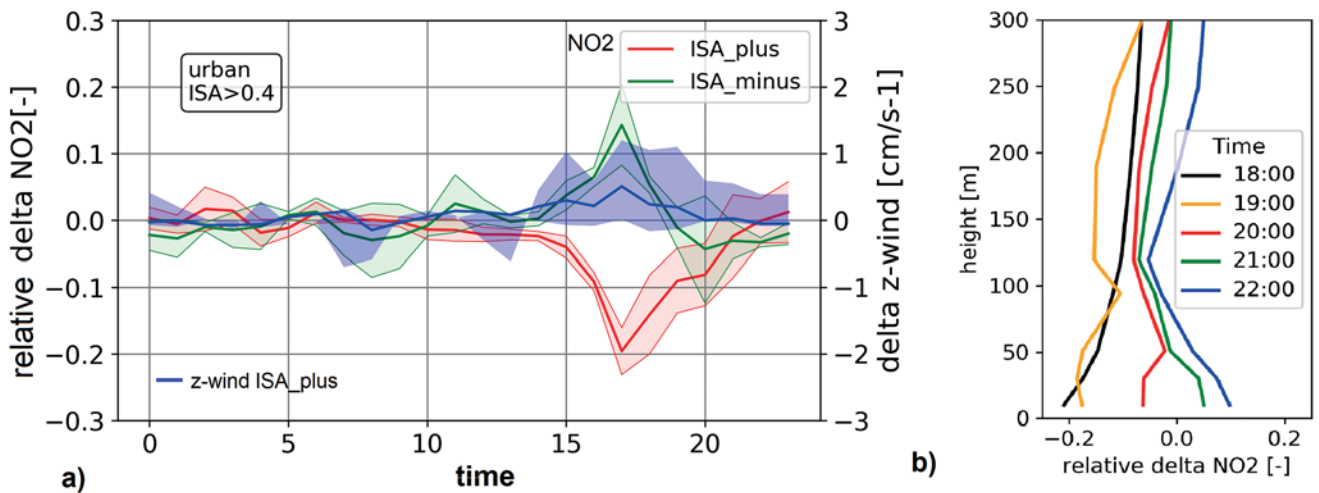


Figure 12: Diurnal mean of relative change in NO₂ presented as difference ISA_minus-BASE (green), ISA_plus-BASE (red) extracted for the Rhine-Main urban area (a) (bold contour in Fig. 7a) Blue line displays difference in vertical velocity between ISA_plus and BASE at the lowest model level, Shading indicates hourly variation for the 10 day model period. Daily mean over 5 simulated hours of vertical profiles for the difference ISA_plus-BASE (averaged over bold contour of Fig. 7a) for the lowest 7 model levels (b) indicating the evening/night-time blocking in a denser urban canyon.

depth study of this aspect is not part of that paper, but needs to be considered in future perspectives. The interaction between dynamics and air chemistry as presented in this chapter is in line with other studies in that field (e.g. SARRAT et al., 2006; LAI and CHENG, 2009; FALLMANN et al., 2016; YUAN et al., 2018)

4 Conclusions

Results from that study show that a sophisticated representation of the urban canopy reduces the mean biases for air temperature and NO₂ concentration between urban background point observations and model grid cell for the episode 1–10 July 2018. These assumptions are validated using a state-of-the-art chemistry-climate model, coupled to the urban canopy parametrization TERRA_URB. As such, sensitivity tests were performed, comparing simulations with (BASE) and without (NO_URB) specific canopy parametrization.

Spatially, the simulation of the surface urban heat island in the model area Frankfurt-Rhein-Main (FRM) for a selected day and time (4 July 2018 21:15) was improved when using TERRA_URB as compared to satellite observation. Adding radiometer measurements, we conclude, that the implementation of an urban canopy parametrization influences surface variables with regard to both dynamic and chemical aspects as well as urban boundary layer properties on a regional scale. Due to a coarse resolution of the model and the underlying emission data set, the system is not able to account for local scale features in an urban environment. The mean meteorological and air chemical conditions for an urban background however were simulated with lower biases as if no urban canopy model was used. Yet, the general bias reduction in temperature and NO₂ between model

and observation shows the benefits of TERRA_URB, being limited to this time period, model domain and setup particularly. In the vertical, we notice an impact of the urban canopy up to a height of about 1000 m within the daytime urban boundary layer and between 200 and 400 m at night, which is in line with observations for other cities. Bias reduction is larger at night-time, because TERRA_URB improves the formulation of the urban energy balance – particularly with regard to a reduced sensible heat loss at night. The sensitivity analysis showed, that the impact of TERRA_URB is most pronounced for high imperviousness, with maximum differences of 1.5 K for surface and 0.6 K for air temperature respectively when comparing an urbanized (BASE) and a configuration without explicit urban parametrization scheme.

The model setup allows for further sensitivity experiments including projected pathways of future urban development in the breadth of increasing population. The difference between a densified and an open space urban landscape is well manifested in the dynamics and chemical properties of the urban boundary layer (0–1000 m). Simulations show a difference in diurnal mean temperature up to 1.5 K at the surface with effects notable up to approximately 300 m with still about 0.3 K. This excess of heat at the surface leads to modified dynamics in the urban boundary layer and triggers upward motion of urban air due to vertical turbulent mixing. This upward motion results in a decrease of daily mean NO₂ concentration from 10–30 %. Vertical transport of pollutants within the urban boundary layer leads to a general decrease over the entire lowermost urban atmospheric column (0–500 m). Above that level, we find that the impact of surface modifications are less pronounced and background effects due to advection from the surrounding are present. Surface to boundary layer cou-

pling is manifested by the urban air warming at a maximum rate of 0.2 K per 0.8 K increase in surface temperature. Per 10 % change in imperviousness, simulations show an increase of 0.17 K for surface- and 0.05 K for air temperature respectively. These values however seem to be low absolutely, model results expect a relative change of NO₂ concentration in the order of 20 %, with a reduction for a temperature increasing (ISA_plus) and an increase for a temperature decreasing scenario (ISA_minus) respectively. A negative side effect of a denser canyon in ISA_plus however results in a temporary relative increase of NO₂ near surface concentration in the evening and night-time, when vertical mixing diminishes and pollutants are emitted into a relatively denser urban canyon.

It has to be noted however, that only using NO₂ concentration as reference might not be enough for revealing the full width of chemistry-dynamics interactions in urban areas. Furthermore, potential chemical interactions have not been thoroughly addressed. Focusing on a clear summer period with weak synoptic forcing we potentially select the simplest synoptic setup. Stating however that these periods are particularly prone for the development of extreme heat events, which as such are projected to evolve more often in the future we find such periods relevant for further analysis and representative for a potential climate change scenario.

This study additionally shows, that a measure reducing the excess heat in urban areas, does not necessarily impact the intensity of the urban heat island itself. In terms of heat regulatory measures, using urban (air) temperature alone might be more adequate when discussing mitigation potentials, particularly when the most severe impacts are expected in daytime, during the period of highest human activity. As such, a re-definition of heat mitigation communication in urban planning has to be considered.

Not being able to account for dedicated urban planning measures due to the coarse model resolution, this study however provides insights for high-resolution street scale models and addresses the need for urban canopy parametrization in regional-scale climate chemistry models. We do not aim to provide an in-depth evaluation of the model system, but an extension of the model capabilities to address sensitivities in regional to urban context.

With a growing number of people residing in urban spaces, a relatively smaller fraction of the atmosphere aloft will be available for the uptake of pollutants in the future. In turn, a dilution of near surface pollutants by changed building geometries will not necessarily be the solution to air quality related problems, but has to be accompanied by emission reduction itself. Urban green infrastructure on the other hand is mandatory for heat reduction, air cleaning and quality of life, but if applied inadequately e.g. when hindering air mixing can counteract the positive cooling effect, in case emissions are not reduced at the same time. As already recently addressed by TRIMMEL et al. (2021), rising air temperatures

expected by climate change cannot easily be reduced by measures concerning buildings within the city itself, but need to involve a whole set of measures. Whole city and regional planning efforts have to be combined, in the framework of a coordinated interdisciplinary communication with local stakeholder and the public (FALLMANN and EMEIS, 2020).

Acknowledgements

This study has been funded by the Carl-Zeiss foundation. Parts of this research was conducted using the supercomputer Mogon and/or advisory services offered by Johannes Gutenberg University Mainz (hpc.uni-mainz.de), which is a member of the AHRP (Alliance for High Performance Computing in Rhineland Palatinate, www.ahrp.info) and the Gauss Alliance e.V. The authors gratefully acknowledge the computing time granted on the supercomputer Mogon at Johannes Gutenberg University Mainz (hpc.uni-mainz.de). Special thanks goes to the Environmental Agency Rheinland-Pfalz LFU-RLP and Dr. MATTHIAS VOIGT and Dr. MATTHIAS ZIMMER in particular, providing access to observations in Mainz. VINOD KUMAR acknowledges the Alexander von Humboldt foundation for Postdoctoral fellowship. Authors acknowledge Deutsches Klimarechenzentrum for providing resources for the MECO(n) simulations. We thank ANDREA POZZER for helping with pre-processing of TNO emissions for use in MECO(n) simulations. We further thank ASTRID KERKWEIG for technical help and constructive feedback.

Appendix:

Within this extra chapter, we intend to discuss recent suggestions by MARTILLI et al. (2020) regarding the use of the term ‘urban heat island’ for assessing heat mitigation potentials for climate sensitive urban planning strategies such as urban greening. It is stated, that a measure reducing the excess heat in urban areas, does not necessarily lead to impacting the intensity of the urban heat island itself. In terms of heat regulatory measures, the authors suggest using urban (air) temperature alone when discussing mitigation potentials, particularly when the most severe impacts are expected in daytime, during the period of highest human activity. In order to entangle the relation between temperature and urban heat island, various urban areas within the model domain (Fig. 2b) have been selected and the impact of the urban planning scenario on both urban heat island and urban temperature has been correlated (Figure A.1a,b). In terms of surface temperature, a cooling largely controls the decrease of urban heat island intensity, with urban areas represented by all grid cells with ISA[0.4;1.0] and rural areas including all grid cells with ISA[0;0.1]. The intensity differs between each urban area ranging from about -0.75 (Zurich) to -2.0 °C (Freiburg) (Figure A.1a). Fig. A.1b on the other hand side suggests, that

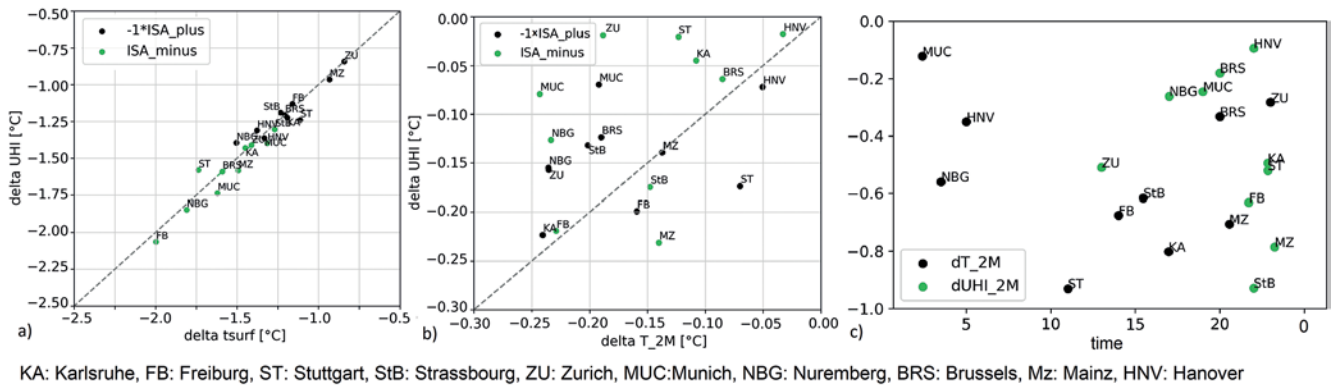


Figure A.1: Correlation between difference in surface (a) and 2 m air temperature (b) for ISA_minus-BASE (gray) and $-1 \times$ ISA_plus-BASE (black) and difference in surface (a) and canopy (b) urban heat island. Hour of the day where maximum effect of urban greening scenario ISA_minus (largest negative difference ISA_minus-BASE) is reached, calculated from daily averages with black being air temperature and green being urban heat island difference.

Table A.1: Sury Input Parameters adapted from (LORIDAN and GRIMMOND, 2012).

urban canopy parameters (inout for SURY)	
parameter	default value
substrate albedo α	0.101
substrate emissivity ϵ	0.86
substrate heat conductivity λ	$0.777 \text{ W m}^{-1} \text{ K}^{-1}$
substrate heat capacity C	$1.25 \times 10^6 \text{ J m}^{-3} \text{ K}^{-1}$
mean building height H	15 m
canyon height-to-width ratio H/W	1.5
roof fraction R	0.667

Table A.2: Urban background stations for evaluation.

Name	measurement height	Location
Stuttgart	3.5 m	$8^\circ 27' 55.01''$, $49^\circ 32' 38.68''$
Freiburg	3.5 m	$7^\circ 49' 55.63''$, $48^\circ 00' 05.46''$
Heidelberg	3.5 m	$8^\circ 43' 0''$, $49^\circ 25' 0''$
Karlsruhe	3.5 m	$8^\circ 24' 14.23''$, $49^\circ 0' 33.16''$
Mannheim	3.5 m	$8^\circ 27' 58''$, $49^\circ 29' 16''$
Mainz	5 m	$8^\circ 16' 0''$, $49^\circ 59' 0''$

an increase in air temperature does not necessarily evoke a linearly corresponding increase in UHI and vice versa, which is indicated by a broader scatter around 1–1. The different features of urban regions are depicted in Figure A.1c, showing the maximum reduction of 2 m temperature (black) and canopy UHI (grey) caused by additional urban green areas in the scenario ISA_minus.

While some areas (ST, FB, STB, KA – green boxes in Fig. 2b) encounter maximum differences of air temperature during the daytime and UHI at night, other areas such as Munich, Hanover and Nuremberg (black boxes in Fig. 2) show an effect slightly shifted towards the night. A slight tendency is found for urban areas in the southern Rhine Valley (green boxes in Fig. 2), stating that particularly here, the discussion of urban heat mitigation strategies has to be focused on the daytime tem-

peratures rather than the urban heat island. For Brussels and Mainz (BRS, MZ – blue boxes) peaks are found at similar times of the day, while Zurich (ZU) shows a reversed tendency. [TableA2]

References

- ACHAKULWISUT, P., M. BRAUER, P. HYSTAD, S.C. ANENBERG, 2019: Global, national, and urban burdens of paediatric asthma incidence attributable to ambient NO₂ pollution: estimates from global datasets. – *The Lancet Planetary Health* 3, e166–e178.
- AMOUEI TORKMAHALLEH, M., Z. AKHMETVALIYeva, A.D. OMRAN, F. FAEZEH DARVISH OMRAN, M. KAZEMITABAR, M. NASERI, M. NASERI, H. SHARIFI, M. MALEKIPIRBAZARI, E. KWASI ADOTEY, S. GORJINEZHAD, N. EGHTEsADI, S. SABANOV, A. ALASTUEY, M. DE FÁTIMA ANDRADE, G. BUONANNO, S. CARBONE, D.E. CÁRDENAS-FUENTES, F.R. CASSEE, Q. DAI, A. HENRÍQUEZ, P.K. HOPKE, P. KERONEN, H.A. KHWAJA, J. KIM, M. KULMALA, P. KUMAR, J. KUSHTA, J. KUULA, J. MASSAGUÉ, T. MITCHELL, D. MOOIBROEK, L. MORAWSKA, J.V. NIEMI, S.H. NGAGINE, M. NORMAN, B. OYAMA, P. OYOLA, F. ÖZTÜRK, T. PETÄJÄ, X. QUEROL, Y. RASHIDI, F. REYES, M. ROSS-JONES, T. SALTHAMMER, C. SAVVIDES, L. STABILE, K. SJÖBERG, K. SÖDERLUND, R. SUNDER RAMAN, H. TIMONEN, M. UMEZAWA, M. VIANA, S. XIE, 2021: Global Air Quality and COVID-19 Pandemic: Do We Breathe Cleaner Air? – *Aerosol Air Qual. Res.* 21, 200567. <https://aaqr.org/articles/aaqr-20-09-covid-0567>.
- BENISTON, M., D.B. STEPHENSON, O.B. CHRISTENSEN, C.A.T. FERRO, C. FREI, S. GOYETTE, K. HALSNAES, T. HOLT, K. JYLHÄ, B. KOFFI, 2007: Future extreme events in European climate: an exploration of regional climate model projections. – *Climatic change* 81, 71–95.
- BRUTSAERT, W., 1982. *Evaporation into the Atmosphere: Theory, History, and Applications*. – Dordrecht, Holland: Reidel, Springer.
- BUETTNER, G., 2004. The CORINE land cover 2000 project. – http://eproceedings.uni-oldenburg.de/website/vol03_3/03_3_buttner2.pdf.
- CARVALHO, D., H. MARTINS, M. MARTA-ALMEIDA, A. ROCHA, C. BORREGO, 2017: Urban resilience to future urban heat waves under a climate change scenario: A case study for Porto urban area (Portugal). – *Urban Climate* 19, 1–27.

- CHANG, Y., J. XIAO, X. LI, S. FROLKING, D. ZHOU, A. SCHNEIDER, Q. WENG, P. YU, X. WANG, X. LI, S. LIU, Y. WU, 2021: Exploring diurnal cycles of surface urban heat island intensity in Boston with land surface temperature data derived from GOES-R geostationary satellites. – *Sci. Total Env.* **763**, 144224. <https://www.sciencedirect.com/science/article/pii/S004896972037755X>.
- DEFRA, 2005. Report: Conversion Factors between ppb and $\mu\text{g m}^{-3}$ and ppm and mg m^{-3} – Defra, UK. https://uk-air.defra.gov.uk/library/reports?report_id=306. Accessed 20 April 2021.
- DEMUZERE, M., K. DE RIDDER, N.P. VAN LIPZIG, 2008: Modeling the energy balance in Marseille: Sensitivity to roughness length parameterizations and thermal admittance. – *J. Geophys. Res. Atmos.* **113**, D16.
- DEMUZERE, M., S. HARSHAN, L. JÄRVI, M. ROTH, C.S. GRIMMOND, V. MASSON, K.W. OLESON, E. VELASCO, H. WOUTERS, 2017: Impact of urban canopy models and external parameters on the modelled urban energy balance in a tropical city. – *Quart. J. Roy. Meteor. Soc.* **143**, 704, 1581–1596.
- DE RIDDER, K., C. BERTRAND, G. CASANOVA, W. LEFEBVRE, 2012: Exploring a new method for the retrieval of urban thermophysical properties using thermal infrared remote sensing and deterministic modeling. *Journal of Geophysical Research: Atmospheres* **117**, D17.
- DIETMÜLLER, S., P. JÖCKEL, H. TOST, M. KUNZE, C. GELLHORN, S. BRINKOP, C. FRÖMMING, M. PONATER, B. STEIL, A. LAUER, J. HENDRICKS, 2016: A new radiation infrastructure for the Modular Earth Submodel System (MESSy, based on version 2.51). – *Geosci. Model Dev.* **9**, 6, 2209–2222. <https://gmd.copernicus.org/articles/9/2209/2016/>.
- DOMS, G., 2011. A description of the nonhydrostatic regional COSMO model. – Part II: Physical parameterization.
- EL-GHAZOUANI, L., A. OUHECHOU, V. HAMOUD, K. KHOMSI, M. MANSOUR, H. RADOIANE, N. LAAROSSI, 2019: The Interaction between Urban Heat Island and Air Quality in Casablanca. – In: 7th International Renewable and Sustainable Energy Conference 2019 (IRSEC), 1–5.
- EMEIS, S., K. SCHÄFER, 2006: Remote Sensing Methods to Investigate Boundary-layer Structures relevant to Air Pollution in Cities. – *Bound.-Layer Meteor.* **121**, 2, 377–385.
- FALLMANN, J., S. EMEIS, 2020: How to bring urban and global climate studies together with urban planning and architecture? – *Developments in the Built Environment* **4**, 100023. <https://www.sciencedirect.com/science/article/pii/S2666165920300193>.
- FALLMANN, J., R. FORKEL, S. EMEIS, 2016: Secondary effects of urban heat island mitigation measures on air quality. – *Atmos. Env.* **125**, 199–211. <http://www.sciencedirect.com/science/article/pii/S1352231015305094>.
- FALLMANN, J., S. WAGNER, S. EMEIS, 2017: High resolution climate projections to assess the future vulnerability of European urban areas to climatological extreme events. – *Theor. Appl. Climatol.* **127**, 667–683.
- GEISS, A., M. WIEGNER, B. BONN, K. SCHÄFER, R. FORKEL, E. VON SCHNEIDEMESSER, C. MÜNDEL, K.L. CHAN, R. NOTHARD, 2017: Mixing layer height as an indicator for urban air quality? – *Atmos. Meas. Tech.* **10**, 2969–2988. <https://amt.copernicus.org/articles/10/2969/2017/>.
- GEORGESCU, M., M. MOUSTAOU, A. MAHALOV, J. DUDHIA, 2013: Summer-time climate impacts of projected megapolitan expansion in Arizona. – *Nature Climate Change* **3**, 37–41.
- GONZALES-ORTIZ, A., 2019: Air Quality in Europe-2019 Report. – European Environment Agency, Luxembourg.
- GRASSELLT, R., D. SCHÜTTEMEYER, K. WARRACH-SAGI, F. AMENT, C. SIMMER, 2008: Validation of TERRA-ML with discharge measurements. – *Meteorol. Z.* **17**, 763–773.
- HAALAND, C., C.K. VAN DEN BOSCH, 2015: Challenges and strategies for urban green-space planning in cities undergoing densification: A review. – *Urban Forestry Urban Greening* **14**, 760–771. <http://www.sciencedirect.com/science/article/pii/S161886671500103X>.
- HAYHOE, K., S. SHERIDAN, L. KALKSTEIN, S. GREENE, 2010: Climate change, heat waves, and mortality projections for Chicago. – *J. Great Lakes Res.* **36**, 65–73.
- HEWITT, C.N., K. ASHWORTH, A.R. MACKENZIE, 2020: Using green infrastructure to improve urban air quality (GI4AQ). – *Ambio* **49**, 62–73.
- HOFMANN, C., A. KERKWEG, H. WERNLI, P. JÖCKEL, 2012: The 1-way on-line coupled atmospheric chemistry model system MECO (n)-Part 3: Meteorological evaluation of the on-line coupled system. – *Geosci. Model Develop.* **5**, 129–147.
- JÖCKEL, P., H. TOST, A. POZZER, C. BRÜHL, J. BUCHHOLZ, L. GANZVELD, P. HOOR, A. KERKWEG, M.G. LAWRENCE, R. SANDER, B. STEIL, G. STILLER, M. TANARHTE, D. TARABORRELLI, J. VAN AARDENNE, J. LELIEVELD, 2006: The atmospheric chemistry general circulation model ECHAM5/MESSy1: consistent simulation of ozone from the surface to the mesosphere. – *Atmos. Chem. Phys.* **6**, 5067–5104. <https://acp.copernicus.org/articles/6/5067/2006/>.
- JÖCKEL, P., A. KERKWEG, A. POZZER, R. SANDER, H. TOST, H. RIEDE, A. BAUMGAERTNER, S. GROMOV, B. KERN, 2010: Development cycle 2 of the Modular Earth Submodel System (MESSy2). – *Geosci. Model Dev.* **3**, 717–752. <https://gmd.copernicus.org/articles/3/717/2010/>.
- JÖCKEL, P., H. TOST, A. POZZER, M. KUNZE, O. KIRNER, C. BRENNINKMEIJER, S. BRINKOP, D.S. CAI, C. DYROFF, J. ECKSTEIN, F. FRANK, H. GARNY, K.-D. GOTTSCHALDT, P. GRAF, V. GREWE, A. KERKWEG, B. KERN, S. MATTHES, M. MERTENS, S. MEUL, M. NEUMAIER, M. NÜTZEL, S. OBERLÄNDER-HAYN, R. RUHNKE, T. RUNDE, R. SANDER, D. SCHARFFE, A. ZAHN, 2016: Earth System Chemistry integrated Modelling (ESCiMo) with the Modular Earth Submodel System (MESSy) version 2.51. – *Geosci. Model Dev.* **9**, 1153–1200.
- JONES, B., B.C. O’NEILL, L. MCDANIEL, S. MCGINNIS, L.O. MEARNS, C. TEBALDI, 2015: Future population exposure to US heat extremes. – *Nature Climate Change* **5**, 652–655.
- KANDA, M., M. KANEGA, T. KAWAI, R. MORIWAKI, H. SUGAWARA, 2007: Roughness lengths for momentum and heat derived from outdoor urban scale models. – *J. Appl. Meteor. Climatol.* **46**, 1067–1079.
- KELLY, F.J., 2019: Urban air quality and health: two steps forward, one step back. – *European Respiratory J.* **53**, 1900280.
- KERKWEG, A., P. JÖCKEL, 2011: The 1-way on-line coupled atmospheric chemistry model system MECO (n)-Part 2: On-line coupling. – *GMDD* **4**, 1359–1402.
- KERKWEG, A., P. JÖCKEL, 2012a: The 1-way on-line coupled atmospheric chemistry model system MECO (n)-Part 1: Description of the limited-area atmospheric chemistry model COSMO/MESSy. – *Geosci. Model Develop.* **5**, 87–110.
- KERKWEG, A., P. JÖCKEL, 2012b: The 1-way on-line coupled atmospheric chemistry model system MECO (n)-Part 2: On-line coupling with the Multi-Model-Driver (MMD). – *Geosci. Model Develop.* **5**, 111–128.
- KERKWEG, A., C. HOFMANN, P. JÖCKEL, M. MERTENS, G. PANTE, 2018. The on-line coupled atmospheric chemistry model system MECO (n)-Part 5: Expanding the Multi-Model-Driver (MMD v2.0) for 2-way data exchange including data interpolation via GRID (v1.0). *Geosci. Model Develop.* **11**, pp. 1059–1076.
- KUENEN, J.J.P., A.J.H. VISSCHEDIJK, M. JOZWICKA, H.A.C. VAN DER DENIER GON, 2014: TNO-MACC_II emission inventory, a multi-year (2003–2009) consistent high-resolution Eu-

- ropean emission inventory for air quality modelling. – Atmos. Chem. Phys. **14**, 10963–10976. <https://acp.copernicus.org/articles/14/10963/2014/>.
- LAFORE, J.P., J. STEIN, N. ASENCIO, P. BOUGEAULT, V. DUCROCQ, J. DURON, C. FISCHER, P. HÉREIL, P. MASCART, V. MASSON, J.P. PINTY, J.L. REDELSPERGER, E. RICHARD, J.V.-G. DE ARELLANO, 1997: The Meso-NH Atmospheric Simulation System. Part I: adiabatic formulation and control simulations. – Ann. Geophysicae **16**, 90–109.
- LAI, L.-W., W.-L. CHENG, 2009: Air quality influenced by urban heat island coupled with synoptic weather patterns. – Sci. The Total Env. **407**, 2724–2733. <http://www.sciencedirect.com/science/article/pii/S0048969708012576>.
- LAMARQUE, J.-F., T.C. BOND, V. EYRING, C. GRANIER, A. HEIL, Z. KLIMONT, D. LEE, C. LIOUSSE, A. MIEVILLE, B. OWEN, M.G. SCHULTZ, D. SHINDELL, S.J. SMITH, E. STEHFEST, J. VAN AARDENNE, O.R. COOPER, M. KAINUMA, N. MAHOWALD, J.R. MCCONNELL, V. NAIK, K. RIAHI, D.P. VAN VUUREN, 2010: Historical (1850–2000) gridded anthropogenic and biomass burning emissions of reactive gases and aerosols: methodology and application. – Atmos. Chem. Phys. **10**, 7017–7039. <https://acp.copernicus.org/articles/10/7017/2010/>.
- LANDESAMT FUER UMWELT RHEINLAND PFALZ, 2018: ZIMEN-Monatsbericht 2018. – Monatsbericht Juli 2018, Zentrales Immissionsmessnetz – ZIMEN. https://luft.rlp.de/fileadmin/luft/ZIMEN/Monatsberichte/2018/ZIMEN-Monatsbericht_2018-7.pdf.
- LANDGRAF, J., P.J. CRUTZEN, 1998: An efficient method for online calculations of photolysis and heating rates. – J. Atmos. Sci. **55**, 863–878.
- LEUKAUF, D., A. GOHM, M.W. ROTACH, 2016: Quantifying horizontal and vertical tracer mass fluxes in an idealized valley during daytime. – Atmos. Chem. Phys. **16**, 13049–13066.
- LORENTE, A., K.F. BOERSMA, H.J. ESKEs, J.P. VEEFKIND, J. VAN GEFFEN, M.B. DE ZEEUW, H.D. VAN DER GON, S. BEIRLE, M.C. KROL, 2019: Quantification of nitrogen oxides emissions from build-up of pollution over Paris with TROPOMI. – Sci. Reports **9**, 1–10.
- LORIDAN, T., C.S. GRIMMOND, 2012: Multi-site evaluation of an urban land-surface model: intra-urban heterogeneity, seasonality and parameter complexity requirements. – Quart. J. Roy. Meteor. Soc. **138**, 1094–1113.
- MAKAR, P.A., S. GRAVEL, V. CHIRKOV, K.B. STRAWBRIDGE, F. FROUDE, J. ARNOLD, J. BROOK, 2006: Heat flux, urban properties, and regional weather. – Atmos. Env. **40**, 2750–2766. <http://www.sciencedirect.com/science/article/pii/S1352231006000264>.
- MARTILLI, A., E.S. KRAYENHOFF, N. NAZARIAN, 2020: Is the urban heat island intensity relevant for heat mitigation studies? – Urban Climate **31**, 100541.
- MASSON, V., 2006: Urban surface modeling and the meso-scale impact of cities. – Theor. Appl. Climatol. **84**, 35–45.
- MAUCHA, G., G. BÜTTNER, B. KOSZTRA, 2010: European validation of GMES FTS SoilSealing Enhancement Data, Final Draft. – EEA. https://www.eea.europa.eu/data-and-maps/data/eea-fast-track-service-precursor-on-land-monitoring-degree-of-soil-sealing/eea-ftsp-degree-of-soil-sealing-1/soilsealing_european_validation_finaldraft2t.pdf, assessed online 3.8.2020.
- MCCARTHY, M.P., M.J. BEST, R.A. BETTS, 2010: Climate change in cities due to global warming and urban effects. – Geophys. Res. Lett. **37**, 9.
- MERTENS, M., A. KERKWEg, P. JÖCKEL, H. TOST, C. HOFMANN, 2016: The 1-way on-line coupled model system MECO (n)-Part 4: Chemical evaluation (based on MESSy v2. 52). – Geosci. Model Develop., published online. <https://iopscience.iop.org/article/10.1088/1748-9326/abf191>.
- MERTENS, M., P. JÖCKEL, S. MATTHES, M. NÜTZEL, V. GREWE, R. SAUSEN, 2021: COVID-19 induced lower-tropospheric ozone changes. – Env. Res. Lett., published online. <https://iopscience.iop.org/article/10.1088/1748-9326/abf191>.
- MUELLER, B., S.I. SENEVIRATNE, 2012: Hot days induced by precipitation deficits at the global scale. – Proceedings of the national academy of sciences **109**, 12398–12403.
- MUSSETTI, G., D. BRUNNER, J. ALLEGRI, A. WICKI, S. SCHUBERT, J. CARMELIET, 2020: Simulating urban climate at sub-kilometre scale for representing the intra-urban variability of Zurich, Switzerland. – Int. J. Climatol. **40**, 458–476.
- NOWAK, D.J., E.J. GREENFIELD, 2020: The increase of impervious cover and decrease of tree cover within urban areas globally (2012–2017). – Urban Forestry Urban Greening **49**, 126638.
- PÖSCHL, U., R. VON KUHLMANN, N. POISSON, P.J. CRUTZEN, 2000: Development and Intercomparison of Condensed Isoprene Oxidation Mechanisms for Global Atmospheric Modeling. – J. Atmos. Chem. **37**, 29–52.
- POZZER, A., P. JÖCKEL, R. SANDER, J. WILLIAMS, L. GANZVELD, J. LELIEVELD, 2006: Technical Note: The MESSy-submodel AIRSEA calculating the air-sea exchange of chemical species. – Atmos. Chem. Phys. **6**, 5435–5444. <https://acp.copernicus.org/articles/6/5435/2006/>.
- PRINGLE, K.J., H. TOST, S. MESSAGE, B. STEIL, D. GIANNAKAKI, A. NENES, C. FOUNTOUKIS, P. STIER, E. VIGNATI, J. LELIEVELD, 2010: Description and evaluation of GMXe: a new aerosol submodel for global simulations (v1). – Geosci. Model Dev. **3**, 391–412. <https://gmd.copernicus.org/articles/3/391/2010/>.
- ROCKEL, B., A. WILL, A. HENSE, 2008: The regional climate model COSMO-CLM (CCLM). – Meteorol. Z. **17**, 347–348.
- ROECKNER, E., R. BROKOPF, M. ESCH, M. GIORGETTA, S. HAGEMANN, L. KORNBUEH, E. MANZINI, U. SCHLESE, U. SCHULZWEIDA, 2006: Sensitivity of Simulated Climate to Horizontal and Vertical Resolution in the ECHAM5 Atmosphere Model. – J. Climate **19**, 3771–3791. https://journals.ametsoc.org/view/journals/clim/19/16/jcli3824.1.xml?tab_body=fulltext-display.
- SANDER, R., A. BAUMGAERTNER, S. GROMOV, H. HARDER, P. JÖCKEL, A. KERKWEg, D. KUBISTIN, E. REGELIN, H. RIEDE, A. SANDU, D. TARABORRELLI, H. TOST, Z.-Q. XIE, 2011: The atmospheric chemistry box model CAABA/MECCA-3.0. – Geoscientific. Model Develop. **4**, 373–380.
- SARKAR, A., K. DE RIDDER, 2011: The Urban Heat Island Intensity of Paris: A Case Study Based on a Simple Urban Surface Parametrization. – Bound.-Layer Meteor. **138**, 511–520.
- SARRAT, C., A. LEMONSU, V. MASSON, D. GUEDALIA, 2006: Impact of urban heat island on regional atmospheric pollution. – Atmos. Env. **40**, 1743–1758.
- SCHAU-NOPPEL, H., M. KOSSMANN, S. BUCHHOLZ, 2020: Meteorological information for climate-proof urban planning – The example of KLIMPRAX. – Urban Climate **32**, 100614.
- SCHULZ, J.-P., G. VOGEL, 2020: Improving the processes in the land surface scheme TERRA: Bare soil evaporation and skin temperature. Atmosphere **11**, 513.
- SCHULZ, J.-P., G. VOGEL, C. BECKER, S. KOTHE, U. RUMMEL, B. AHRENS, 2016: Evaluation of the ground heat flux simulated by a multi-layer land surface scheme using high-quality observations at grass land and bare soil. Meteorol. Z. **25**, 607–620. DOI:10.1127/metz/2016/0537.
- SHARMA, R., H. HOOYBERGHS, D. LAUWAET, K. DE RIDDER, 2019: Urban heat island and future climate change—Implications for Delhi’s heat. – J. Urban Health **96**, 235–251.

- STEPPELER, J., G. DOMS, U. SCHÄTTLER, H.W. BITZER, A. GASSMANN, U. DAMRATH, G. GREGORIC, 2003: Mesogamma scale forecasts using the nonhydrostatic model LM. – *Meteor. Atmos Phys.* **82**, 75–96.
- STROHBACH, M.W., A.O. DÖRING, M. MÖCK, M. SEDREZ, O. MUMM, A.-K. SCHNEIDER, S. WEBER, B. SCHRÖDER, 2019: The “Hidden Urbanization”: Trends of Impervious Surface in Low-Density Housing Developments and Resulting Impacts on the Water Balance. – *Frontier Env. Sci.* **7**, 29. <https://www.frontiersin.org/article/10.3389/fenvs.2019.00029>.
- TOST, H., P. JÖCKEL, A. KERKWEIG, R. SANDER, J. LELIEVELD, 2006: Technical note: A new comprehensive SCAVenging submodel for global atmospheric chemistry modelling. – *Atmos. Chem. Phys.* **6**, 565–574.
- TOST, H., M.G. LAWRENCE, C. BRÜHL, P. JÖCKEL, 2010: Uncertainties in atmospheric chemistry modelling due to convection parameterisations and subsequent scavenging. – *Atmos. Chem. Physics* **10**, 4, 1931–1951.
- TRIMMEL, H., P. WEIHS, S. FAROUX, H. FORMAYER, P. HAMER, K. HASEL, J. LAIMIGHOFER, D. LEIDINGER, V. MASSON, I. NADEEM, S.M. OSWALD, M. REVESZ, R. SCHOETTER, 2021: Thermal conditions during heat waves of a mid-European metropolis under consideration of climate change, urban development scenarios and resilience measures for the mid-21st century. – *Meteorol. Z.* **30**, 9–32. https://www.schweizerbart.de/papers/metz/detail/30/9/1938/Thermal_conditions_during_heat_waves_of_a_mid_European_metropolis_under_consideration_of_climate_change_urban_development_scenarios_and_resilience_measures_for_the_mid_21st_century.
- TRUSILOVA, K., S. SCHUBERT, H. WOUTERS, B. FRÜH, S. GROSSMAN-CLARKE, M. DEMUZERE, P. BECKER, 2016: The urban land use in the COSMO-CLM model: a comparison of three parameterizations for Berlin. – *Meteorol. Z.* **25**, 231–244.
- UMWELTBUNDESAMT, 2019: Struktur der Flächennutzung. – <https://www.umweltbundesamt.de/daten/flaechen-boden-land-oekosysteme/flaechen/struktur-der-flaechennutzung#die-wichtigsten-flaechennutzungen>.
- UNITED NATIONS, 2018: 2018 Revision of World Urbanization Prospects. – <https://population.un.org/wup/>.
- VITERBO, P., A.C.M. BELJAARS, 1995: An improved land surface parameterization scheme in the ECMWF model and its validation. – *J. Climate* **8**, 2716–2748.
- WOUTERS, H., K. DE RIDDER, N.P.M. VAN LIPZIG, 2012: Comprehensive Parametrization of Surface-Layer Transfer Coefficients for Use in Atmospheric Numerical Models. – *Bound.-Layer Meteor.* **145**, 539–550.
- WOUTERS, H., K. DE RIDDER, M. DEMUZERE, D. LAUWAET, N.P.M. VAN LIPZIG, 2013: The diurnal evolution of the urban heat island of Paris: a model-based case study during Summer 2006. – *Atmos. Chem. Phys.* **13**, 8525–8541. <https://acp.copernicus.org/articles/13/8525/2013/>.
- WOUTERS, H., M. DEMUZERE, K. DE RIDDER, N.P. VAN LIPZIG, 2015a: The impact of impervious water-storage parametrization on urban climate modelling. – *Urban Climate* **11**, 24–50.
- WOUTERS, H., M. DEMUZERE, K. DE RIDDER, N.P.M. VAN LIPZIG, 2015b: The impact of impervious water-storage parametrization on urban climate modelling. – *Urban Climate* **11**, 24–50.
- WOUTERS, H., M. DEMUZERE, U. BLAHAK, K. FORTUNIAK, B. MAIHEU, J. CAMPS, D. TIELEMANS, N. VAN LIPZIG, 2016b: The efficient urban canopy dependency parametrization (SURY) v1.0 for atmospheric modelling: description and application with the COSMO-CLM model for a Belgian summer. – *Geosci. Model Develop.* **9**, 3027–3054.
- XIE, X., Z. HUANG, J. WANG, 2005: Impact of building configuration on air quality in street canyon. – *Atmos. Env.* **39**, 4519–4530. <http://www.sciencedirect.com/science/article/pii/S1352231005003596>.
- YUAN, M., Y. SONG, Y. HUANG, S. HONG, L. HUANG, 2018: Exploring the association between urban form and air quality i. – *J. Plan. Education Res.* **38**, 413–426.